Sequence-aware energy consumption prediction for electric vehicles using pre-trip realistically accessible data

Applied Energy 401 (2025) 126673

Contents lists available at ScienceDirect

Applied Energy

journal homepage: www.elsevier.com/locate/apen

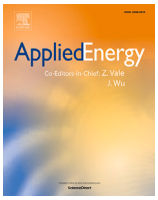

Sequence-aware energy consumption prediction for electric vehicles using pre-trip realistically accessible data

Haichao Huang [a], Kun Gao [b,*], Yizhou Wang [a], Arsalan Najafi [b], Zhe Zhang [a], Hongdi He [a]

[a] School of Ocean and Civil Engineering, Shanghai Jiao Tong University, Shanghai, CN-200240, China
[b] Department of Architecture and Civil Engineering, Chalmers University of Technology, Goteburg, SE-412 96, Sweden

HIGHLIGHTS

- Utilizing realistically accessible pre-trip data rather than assuming unrealistic inputs prior to departure.
- Introduction of a sequence-aware methodology for electric vehicle energy consumption prediction.
- Comprehensive comparison of sequence-aware and non-sequence-aware models across three diverse datasets.
- Quantification of the relationship between segment-level features and energy consumption.

ARTICLE INFO

Keywords:
Energy consumption prediction
Sequence-dependence aware
Realistically accessible data
Deep learning

ABSTRACT

Energy consumption (EC) prediction plays a crucial role in reducing range anxiety and operation scheduling as well as optimization of electric vehicles. Current methods predominantly treat a trip as a singular entity or assume unrealistic inputs (e.g., driving trajectories or speed profiles of a trip) that are not accessible prior to departure for EC prediction. This study proposes a sequence-dependence aware deep learning methodology for EC prediction using pre-trip realistically accessible data. Sequence modeling architectures are employed to capture the nuanced variations and dependencies among adjacent segments rather than relying on coarse-grained average features. This study highly emphasizes pre-trip accessible data in reality for trip EC prediction, improving upon unrealistic assumptions that presuppose access to future speed profiles per second throughout a trip. Large-scale field datasets are utilized for model development, covering 2.2 million kilometers of driving from eight cities and four different vehicle models. The results demonstrate that the proposed sequence-dependence aware deep learning methodologies outperform existing methods in both prediction accuracy and interpretability, highlighting the efficacy of incorporating sequence dependencies in EC prediction. This study also quantifies the influence of various factors on EC at the segment level, providing a more granular analysis and understanding of energy efficiency. The results provide accurate and realistic EC predictions and understanding for electric vehicles that are applicable in real practice.

1. Introduction

The global energy and transportation sectors remain critically dependent on fossil fuels, creating cascading challenges ranging from urban air pollution to climate change mitigation [24,35]. While electric vehicles (EVs) present a promising decarbonization pathway, the adoption of EVs faces a substantial hurdle in the form of range anxiety [19]. Range anxiety refers to the psychological barrier stemming from uncertainties in battery endurance during trips [45]. Automobile manufacturers attempt to mitigate this concern through trip-specific energy consumption (EC) predictions, creating significant demand for robust predictive models that balance accuracy with practical implementability [37]. This dual requirement has fueled growing interest in data-driven approaches that leverage real-world operational data while maintaining computational feasibility [1].

Current EC prediction methodologies exhibit two fundamental limitations that constrain their practical utility. First, certain approaches [4,15,36] achieve impressive precision through theoretical assumptions requiring predictive or clairvoyant access to second-resolution speed

* Corresponding author.
Email address: gkun@chalmers.se (K. Gao).

https://doi.org/10.1016/j.apenergy.2025.126673
Received 17 March 2025; Received in revised form 7 July 2025; Accepted 20 August 2025
Available online 2 September 2025

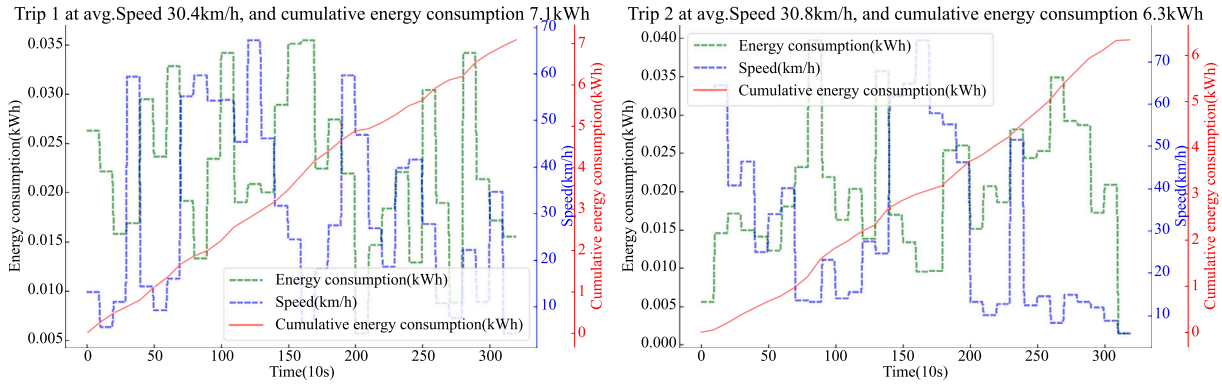

Fig. 1. Speed profiles and the EC on two real trips.

profiles. While these models demonstrate technical sophistication, the inherent complexity of real-world traffic conditions and the computational impracticality of forecasting high-resolution velocity–acceleration sequences render them infeasible for practical implementation. Conversely, alternative implementations [6,28,40] employ oversimplified trip-level averaging data that fundamentally disregard sequential speed dynamics along the pathway, thereby introducing systematic errors in energy prediction. This fundamental limitation underscores a critical knowledge gap in modeling approaches that fail to account for sequential dependencies – a crucial factor substantially influencing EC. Our analysis reveals compelling evidence through comparative case studies: As demonstrated in Fig. 1, two comparable trips exhibit a 12.7 % divergence in total EC (7.1 kWh vs. 6.3 kWh) despite nearly identical average speeds (30.4 vs. 30.8 km/h) and external environmental factors. This empirical evidence quantitatively establishes that conventional average-speed-based models inherently neglect the critical impact of sequence patterns on EC.

Addressing this knowledge gap, this study endeavors to propose a sequence-aware deep learning framework for EC prediction using exclusively and realistically pre-trip accessible data. It is imperative to underscore that the primary distinction of our study from previous research lies in the grounding of relaxing the unrealistic assumptions of presupposing access to future speed profiles (specifically, speed per second over the course of a future trip) in real traffic environments. Instead, this study takes the pre-trip and practically obtainable data from map navigation applications (e.g., Google Maps) as inputs to predict EC, including the road-segment average speed in the planned route for a trip. Additionally, in contrast to prior studies [22,32], our methodology is built upon a more extensive and diverse dataset, encompassing environmental factors and electric vehicle data of eight cities. The dataset is compiled from four different vehicle models and over 2.2 million kilometers of driving, thereby enhancing its applicability and generalizability. The main contributions of this study can be summarized as follows:

1. This study eschews the unrealistic assumptions of presupposing access to future speed profiles per second over the course of a future trip-in real traffic environments. Instead, our model leverages realistically obtainable data from map navigation applications to predict EC.
2. This study introduces a sequence-aware methodology for EC prediction. By discretizing trips into ordered segments, EC prediction is conceptualized as a sequential prediction task. Sequence modeling architectures can capture the nuanced variations among adjacent segments rather than relying on coarse-grained average features.
3. This study conducts a comprehensive comparative analysis of the efficacy between sequence-aware models and non-sequence-aware models across three diverse datasets, aiming to validate the significance of sequence dependence considerations and the generalizability of the methodologies.
4. This study provides empirical insights into the nuanced impact of various features on EC at the segment level rather than a coarse trip-level analysis, providing a more granular analysis that enhances the understanding of energy efficiency and facilitates the development of advanced eco-driving strategies.

The remainder of this paper is organized as follows. Section 2 reviews the literature and analyzes the research gaps in previous studies. Section 3 describes the data preprocessing and clarifies methodologies. Section 4 presents the analysis results. Finally, Section 5 discusses and concludes the paper.

2. Literature review

The development of precise and widely applicable EC prediction approaches is paramount in alleviating driver range anxiety. Consequently, considerable effort has been directed towards devising approaches for predicting trip EC. These approaches can be broadly classified into two categories: model-based and data-driven approaches.

Model-based approaches involve the establishment of simulation models grounded in vehicle dynamics and kinematics, aiming at discerning the impact of external and transmission system parameters on EC across diverse conditions [20,41,42]. [44] proposed a simulation-based quasi-statistical method to predict electric vehicle energy usage in a large-scale network under various road vehicle operating conditions. [16] used a transient simulation model to calculate and quantify the electrical energy demand of a vehicle for a given change in travel period, direction, altitude, and ambient temperature during a trip. [29] proposed a combination of a physically based model and a machine learning model, where the mechanical power is calculated using physical formulas and the machine learning model is used to estimate the mapping relationship between mechanical power and electrical power. [25] discussed the influence of lateral dynamics on the EC of electric vehicles, which improved the accuracy and reliability of EC prediction. [47] proposed a minimum equivalent fuel consumption model that provided longitudinal force distribution control outcomes for predicting EC in hybrid electric vehicles. However, model-based approaches rely on high-fidelity parameter configuration, resulting in a lack of broad applicability [50] and pose challenges in large-scale and real-world assessments [49].

Data-driven approaches have piqued the interest of service providers due to their applicability and potential for large-scale deployment [14,18]. These approaches involve constructing predictive models for EC based on influential factors, utilizing extensive real-world driving data from EVs [36]. Many innovative models have been proposed and have demonstrated the effectiveness of data-driven approaches. [46] introduced a machine learning-based EC prediction framework that

incorporated driving condition prediction, achieving a 30 % higher prediction accuracy than traditional methods. [39] compared the advantages and disadvantages of four state-of-the-art machine learning models for EC prediction and explored the relative impact of influential factors on the EC. [7] devised an enhanced density-based clustering multivariate linear regression model for EC prediction. This model automatically captures training features in real-world driving scenarios, showcasing superior prediction accuracy. Despite the commendable prediction accuracy achieved by these methods, they share a limitation in treating a trip as a singular entity and disregarding feature variations throughout the trip.

Some researchers have acknowledged the limitations of current methodologies and have turned their attention to the discourse on EC prediction for segments. [35] formulated a segment-level EC estimation model through decomposition analysis. [34] introduced a probabilistic deep model for predicting segment-level EC. [33] presented a hybrid approach that integrates a short-trip segment division algorithm with deep neural networks to enhance the precision of segment-level EC prediction. Although these studies take into account the feature variations throughout the trip, they treat each segment as an independent entity for prediction, neglecting the interdependencies between adjacent segments. The chronologically ordered segments can be viewed as the time series, and interdependence among the EC in adjacent segments may offer valuable information about EC, potentially contributing to improved EC prediction.

Moreover, the EC is intricately influenced by various factors, posing a significant challenge to EC prediction. The first category comprises intrinsic vehicle-related factors, including speed [36], driver behavior [9], and auxiliary equipment [26]. The second category involves external factors, constituting traffic conditions [30], infrastructure [10,23], and weather [38]. Some studies analyze the impact of different factors on EC, providing valuable insights for more accurate EC prediction. Some of these studies focus on a micro-level analysis of the relationship between influencing factors and EC based on per-second data, while others discuss it from a macro perspective, considering the entire trip. Limited research directly analyzes the relationship between factors and EC from a meso-level (segment-level) perspective. As a result, these conclusions may have limitations when applied to segment-level prediction models.

3. Data and methodology

3.1. Data description

This study utilizes EV datasets from eight cities, shown in Fig. 2. The dataset spans eight cities over a duration of 6 to 12 months. It includes 43 EVs representing four distinct vehicle models, accumulating a total mileage exceeding 2.2 million kilometers. The operational data were collected through in-vehicle T-box devices and transmitted via the Controller Area Network (CAN), adhering to the GB/T 32960.3–2016 transmission protocol. (1) The SHEV dataset, sourced from Shanghai, encompasses operational data from 20 BEIJING EU5 vehicles spanning July 30, 2021, to January 26, 2022, accumulating a travel mileage of 838,753 kilometers. Data are sampled at 10-second intervals, yielding over 15 million operating records. (2) The SZEV dataset, collected in Shenzhen, spans seven months from April 1, 2022, to October 30, 2022. It includes ten vehicles from two models, namely, 5 GAC AION S and 5 BYD SONG, with a cumulative traveled mileage surpassing 680,000 kilometers. The data are sampled at 20-second intervals, amassing over 6 million operating records. (3) The CNEV dataset encompasses eight major cities in China, documenting operational data from 13 FAW EHS-3 vehicles throughout the year 2022, covering a cumulative traveled mileage of 759,099 kilometers. Data are sampled at 10-second intervals, generating over 13 million operating records.

Notably, potential biases are inevitably introduced when collecting data from different cities and vehicle models. Therefore, this study adopted two mitigation measures. First, we synchronously collected environmental data from https://rp5.ru/ to alleviate biases caused by

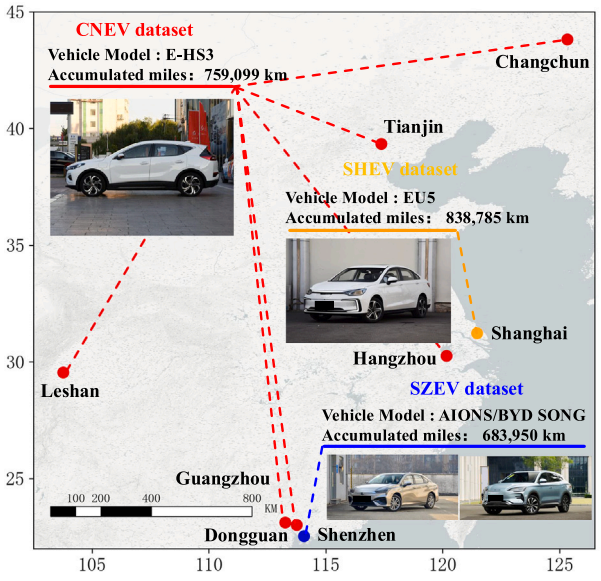

Fig. 2. Description of EV datasets.

Table 1
Descriptive statistics of the datasets.

	SHEV	SZEV	CNEV
Brand	BEIJING EU5	GAC AION S/ BYD SONG Plus	FAW EHS-3
Energy consumption rate (kWh/100 km)	13.3	12.5/14.1	14
Rated Battery capacity (kWh)	50.8	60/87	52.5
Temperature range (°C)	[–2, 35]	[11, 36]	[–4,36]
Accumulated range (km)	92	137	105
Avg. travel time (min)	55	113	79
Avg. travel speed (km/h)	35.5	35.8	39.8
Logging frequency (Hz)	0.1	0.2	0.1
Number of trips	9118	4989	7471
Number of segments	838,785	683,950	759,099

driving conditions and urban climates. Additionally, we performed separate modeling on three datasets to mitigate the biases from driving patterns and vehicle models. However, we must acknowledge that these measures cannot completely eliminate the heterogeneity in the datasets. The performance and generalizability of the models may still be affected by the inherent variations. These factors should be considered in real-world scenario modeling to ensure reliable predictions.

Table 1 provides the descriptive statistics for the three datasets, illustrating variations in vehicle models, ambient temperature, and usage patterns. Overall, this study encompasses 21,278 trips. Examples of the variable fields included in the original datasets are shown in the appendix.

3.2. Data preprocessing and feature formation

3.2.1. Data preprocessing

Data preprocessing includes three key steps: anomaly handling, trip division, and segment division.

Anomaly handling: The data collection and transmission process inherently introduces anomalies, primarily in the form of missing data and outliers. Some outliers may potentially incorporate important data patterns and should not be simply removed. Therefore, only values that are

entirely meaningless, such as placeholder values (e.g., 0xFE or 99999), were considered outliers and removed. Moreover, for isolated outliers, we performed imputation to maintain data continuity. However, for consecutive outliers (e.g., exceeding one minute), we directly removed them to avoid unreasonable data points, as interpolation could lead to significant errors in predicting trip energy consumption. Then, the data underwent imputation using Lagrange interpolation [5] along the time axis, resulting in a refined dataset.

Trip division: The refined dataset, presented as chronologically ordered continuous data, includes non-trip events such as parking and charging. For analysis, we extracted data when the vehicles were operating. A data segment is identified as an independent trip when the time gap between adjacent data points in the driving data exceeds 15 minutes [46]. Trips with distances below 1 km or durations less than 10 minutes are excluded. Additionally, a histogram of the divided trip distances and durations after processing is included in the appendix Fig. S1 to clarify the criteria.

Segment division: The odometer reading field within a dataset serves as a robust foundation for segment division. Odometer reading pertains to the cumulative distance covered by a vehicle, prominently showcased on the dashboard. This metric is derived from monitoring tire rotations, with each revolution incrementally adding to the overall distance traveled. Given that the minimum unit of odometer reading in the dataset is 1 km, the divided trips are thus segmented on a per-kilometer basis. For example, if a trip is 10 km, then the trip is divided into 10 one-kilometer segments that are chronologically ordered. A maximum of 450 segments per trip is set, utilizing zero padding [31] to maintain a consistent data structure for modeling.

The targeted scenario in this study is: when the driver determines the destination on the navigation map, the proposed method integrates trip features from the map navigation, ambient features, and vehicle status features at that moment to predict the EC for the upcoming trip. It is important to highlight that the segmentation thresholds may affect model performance greatly. The choice of a 1 km segmentation threshold was necessitated by the limitations of the current dataset. However, with appropriate datasets, our method can also accommodate finer segmentation thresholds, such as 500 m or 100 m. There are no specific mandates regarding the segmentation threshold within the proposed method. In practical application, the segmentation threshold depends on the map navigation platform that provides the information. For example, Baidu Maps (https://map.baidu.com) furnishes traffic information every 200 m, enabling the segmentation threshold to be adjusted accordingly.

3.2.2. Feature formation

To train the proposed models based on our available data, EC can be calculated by integrating the voltage and current of the EV battery over time (measured in kWh) [48]. The methods for generating these features are elaborated in Table 2.

$$ec^s = \frac{t}{3600} \times \sum_{i=1}^{n} V_i^s I_i^s \times \frac{1}{1000} \qquad i = 1, 2, \ldots, n \tag{1}$$

where ec^s is the energy consumption of the s-th segment, in kWh, V_i and I_i are the battery voltage and current measured at each time step in Volts and Amperes. t is the time step with the unit in seconds, and n is the number of operational records within a segment.

Although driving features are indeterminate before the trip commences, once the trip origin and destination are determined, these features can be acquired through the Application Programming Interface (API) of the map navigation platform, as depicted in Fig. 3. It is one emphasis of the proposed method, namely grounded in realistic and practically attainable data instead of unrealistic high-resolution speed profiles (e.g., at one-second intervals). Driving features encompass characteristics such as distance, duration, and speed of road segments in the route provided by map navigation. Duration signifies the time taken to traverse a segment, measured in minutes, while speed denotes the average speed during the segment.

Table 2
The segment features of a trip.

Category	Features	Processing methods
Target	Energy consumption (kWh)	Eq. (1)
Trip features	Speed (km/h)	Provided by map service API
	Duration (min)	Provided by map service API
	Distance (km)	Provided by map service API
Ambient features	Temperature (°C)	Provided by weather service API
	Wind speed (m/s)	Provided by weather service API
	Season	Spring-Winter→1–4
	Period	Rush hours (7:00–9:00 & 15:00–17:00) nighttime (22:00–6:00) the remaining hours→1–3
	Date	Fri.-Sun.→1–7
Vehicle status feature	DOD (%)	$DOD = 1 - SOC_{init}$
	Remaining warranty utilization rate (%)	$Rate_{RWU} = 1 - M_{cur}/M_{war}$
	Voltage inconsistency (V)	$Vol_{std} = \sqrt{\frac{1}{n} \times \sum_{i=1}^{n} (vol_i - vol_{avg.})}$
	Temperature inconsistency (°C)	$Temp_{std} = \sqrt{\frac{1}{n} \times \sum_{i=1}^{n} (temp_i - temp_{avg.})}$

Ambient features consist of temperature, wind speed, season, period, and date, exerting an indirect influence on EC. For instance, weekdays and rush hours may escalate energy usage due to traffic congestion. Temperature and wind speed data are sourced from https://rp5.ru/ and aligned with the original data based on timestamps, while season, period, and date are numerically encoded. The wind data do not include the relationship between driving direction and wind direction, which is a shortcoming of the data. However, previous studies [11] have shown that wind speed has a positive and statistically significant effect on the ECR without considering the relationship between driving direction and wind direction. Therefore, considering wind could be helpful for energy consumption in the model.

Vehicle status features include Depth of Discharge (DOD), remaining warranty utilization rate, voltage inconsistency, and temperature inconsistency. Remaining warranty utilization rate is the proportion of unused mileage for the remaining warranty period to the maximum mileage guaranteed by the manufacturer, expressed as 1 minus the ratio of the current odometer reading to the maximum warranty mileage. All these factors potentially impact energy usage efficiency and thus impact the real EC during a trip. For instance, a vehicle with a deeper DOD may exhibit distinct EC compared to a fully charged state, and ageing batteries may consume more energy for a trip due to higher resistance inside the battery. Please note that due to some features relying on API calls, an unstable network could adversely affect model performance, potentially rendering it inoperable. Therefore, the model requires a stable network environment to operate effectively.

Importantly, during actual prediction of EC for a trip, ambient features and vehicle status features in the future are unknown. However, considering that except for DOD, other features undergo slight changes throughout a trip. Therefore, the prediction model utilizes the values of the features at the beginning of the trip in our prediction models, which can be obtained in real applications. It is worth noting that this is to avoid training models with high fitness but weak practical applicability, on account that it is not possible to know the exact values of these features for a trip before departure.

Fig. 3. Real-time speed profiles provided by map navigation platform.

Table 3
Variance inflation factor for model features.

Features	SHEV dataset	SZEV dataset	CNEV dataset
Speed	16.01	28.49	5.31
Duration	36.56	58.00	3.64
Distance	36.38	61.67	1.28
Temperature	12.69	50.11	14.00
Wind speed	4.06	4.21	4.99
period	10.50	9.39	6.04
Date	3.20	3.20	3.26
Season	57.93	8.71	7.34
DOD	2.31	2.46	2.96
Remaining warranty utilization rate	119.87	64.81	40.18
Voltage inconsistency	1.11	1.26	2.18
Temperature inconsistency	1.15	12.57	3.58

To identify potential multicollinearity among features, we calculated the variance inflation factor (VIF) for each feature, as shown in Table 3. VIF values exceeding 10 typically indicate significant multicollinearity. Addressing multicollinearity is pivotal in regression analysis as it determines the uniqueness of coefficients. However, for machine learning models focused on prediction, multicollinearity holds less significance because our primary concern is minimizing model prediction loss rather than estimating coefficients [43]. Although its impact on predictive performance is minimal, caution is essential when interpreting machine learning models in the presence of multicollinearity. Multicollinearity can diminish the importance of features that are highly correlated with each other, potentially leading to misleading interpretations and rankings of feature significance. To better understand the potential impact of multicollinearity, several features with high VIF values will be further analyzed in the results section.

VIF is used to diagnose multicollinearity rather than to assess feature importance, as high collinearity among predictors can lead to misleading conclusions in post-hoc analyses. While future work could explore attribution techniques such as Shapley Additive Explanations (SHAP), we caution that these post-hoc methods may obscure the true drivers of EC. For example, distance, speed, and duration are mathematically interdependent, making it difficult for SHAP to assign meaningful independent importance scores. While all three may appear important, distance more directly captures physical EC, whereas duration and speed may act as contextual modifiers (e.g., traffic or driving style). Likewise, ambient temperature and season are strongly correlated—temperature directly affects air conditioning load and battery efficiency, while season serves only as a temporal proxy. Given these challenges, we recommend that the identification of key EC drivers be guided by domain expertise or by decoupling frameworks [49] that explicitly account for confounding influences.

3.3. Modeling approaches

Generally, the segment-level EC prediction can be viewed as a supervised learning problem, where features f_i^s in the segment i within a trip are mapped to the ec_i of the segment.

$$M_\theta : F \subset \mathbb{R}^{N_s \times D_f} \rightarrow \mathbf{E}[ec_1, ec_2, \ldots, ec_N] \subset \mathbb{R} \tag{2}$$

Another straightforward way is a mapping from features of all segments to the total EC on a trip.

$$M_\theta : F \subset \mathbb{R}^{N_s \times D_f} \rightarrow E \subset \mathbb{R} \tag{3}$$

where θ is the learnable parameter of the model. The mapping rules should be learned from real trip data.

$$D = \left\{ (f_{i,j}^s, e_j^s) \mid 1 \le i \le N_f, 1 \le s \le N_s, 1 \le j \le N_t \right\} \tag{4}$$

where $f_{i,j}^s$ denotes the i-th feature in the s-th segment of the j-th trip, e_j^s is the corresponding segment-level energy consumption, N_f is the number of features per segment, N_s is the number of segments per trip, and N_t is the number of trips. Index i refers to feature dimension, s to segment order, and j to trip index.

This study delineates four prediction methods, with their distinctions visually shown in Fig. 4. Whether to consider the sequential interdependencies between adjacent segments in EC prediction categorizes the models into sequential or non-sequential methods. Whether the model outputs a sequence composed of the EC of each segment or the total EC for the entire trip is categorized as segment-accumulation or trip-level.

3.3.1. Sequential prediction

Sequential segment accumulation (SA): For sequential prediction, the input necessitates a 3-D tensor comprising samples, segments, and features. The model not only captures the interdependencies between the current segment and EC but also incorporates the feature information and interdependencies of preceding segments on EC. It sequentially generates the predicted EC for each segment. Then, these predicted segment EC are aggregated to provide the total EC projection for the entire trip. Segment accumulation is formally defined as follows.

$$EC_j^{SA} = \sum_{s=1}^{N_s} M_\theta \left(\begin{bmatrix} f_{1,j}^1 & f_{1,j}^2 & \cdots & f_{1,j}^s \\ f_{2,j}^1 & f_{2,j}^2 & \cdots & f_{2,j}^s \\ \vdots & \vdots & \ddots & \vdots \\ f_{d,j}^1 & f_{d,j}^2 & \cdots & f_{d,j}^s \end{bmatrix} \right) = \sum_{s=1}^{N_s} \left[ec_j^1, ec_j^2, \ldots, ec_j^s \right] \subset \mathbb{R}^{1 \times N_s} \tag{5}$$

Sequential trip-level (ST): This method holds the same mechanism to consider the sequence interdependencies among segments on EC of the trip, but directly predicts the total EC at the trip-level rather than

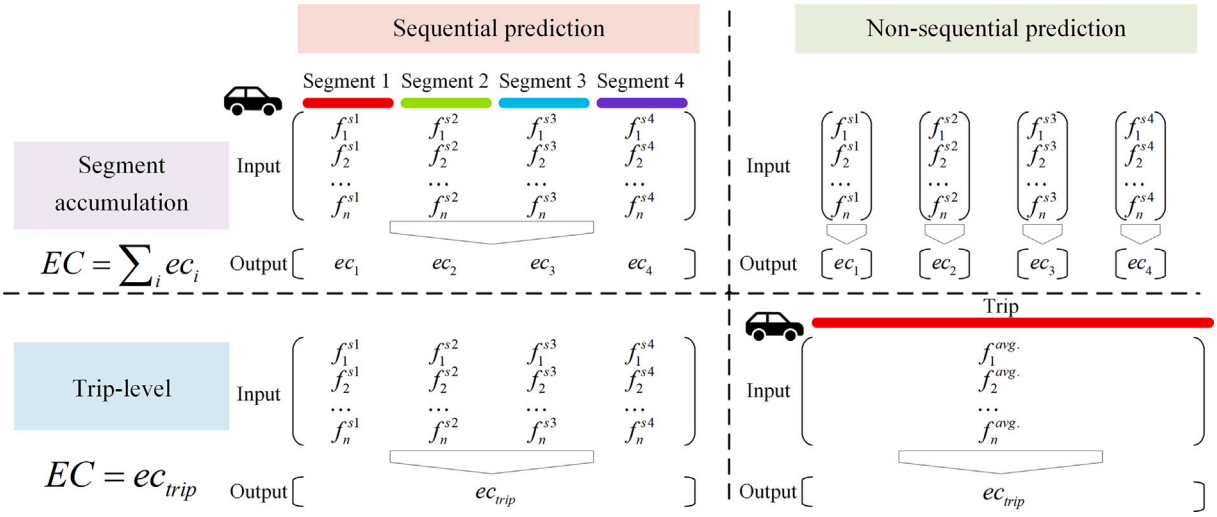

Fig. 4. Diagrammatic interpretation of EC prediction methods.

predicting EC for each segment. The prediction process is mathematically expressed as

$$EC_j^{ST} = \sum_{s=1}^{N_s} M_\theta \left(\begin{bmatrix} f_{1,j}^1 & f_{1,j}^2 & \cdots & f_{1,j}^s \\ f_{2,j}^1 & f_{2,j}^2 & \cdots & f_{2,j}^s \\ \vdots & \vdots & \ddots & \vdots \\ f_{d,j}^1 & f_{d,j}^2 & \cdots & f_{d,j}^s \end{bmatrix} \right) = ec_j \tag{6}$$

3.3.2. Non-sequential prediction

Non-sequential segment accumulation (NSA): For non-sequential prediction, the input is a 2-D tensor consisting of samples and features. NSA, in essence, disregards the sequence interdependence between segments in EC predictions. Instead, it treats the EC prediction for each segment as an independent task. The predicted EC for each segment is computed and aggregated to provide the total EC projection for the entire trip. Its formal definition is as follows.

$$\begin{aligned} EC_j^{NSA} &= \sum_{s=1}^{N_s} CAT \left[M_\theta^1 \left(\begin{bmatrix} f_{1,j}^1 \\ f_{2,j}^1 \\ \vdots \\ f_{d,j}^1 \end{bmatrix} \right), M_\theta^1 \left(\begin{bmatrix} f_{1,j}^2 \\ f_{2,j}^2 \\ \vdots \\ f_{d,j}^2 \end{bmatrix} \right), \ldots, M_\theta^1 \left(\begin{bmatrix} f_{1,j}^s \\ f_{2,j}^s \\ \vdots \\ f_{d,j}^s \end{bmatrix} \right) \right] \\ &= \sum_{s=1}^{N_s} \left[ec^1, ec^2, \ldots, ec^s \right] \end{aligned} \tag{7}$$

Non-sequential trip-level (NST): NST is exactly the traditional method currently deployed for predicting energy consumption based on deep learning methods [12,39]. For comparison purposes, this study defines this method as NST. It utilizes the mean values of features throughout the trip as input, neglecting the variations in features over the trip. The prediction process takes a macroscopic view of EC, and its mathematical expression is given by

$$EC_j^{NT} = M_\theta^1 \left(\begin{bmatrix} f_{1,j}^{avg.} \\ f_{2,j}^{avg.} \\ \vdots \\ f_{d,j}^{avg.} \end{bmatrix} \right) = ec_j \tag{8}$$

3.4. Deep learning models for sequential predictions

From a supervised learning perspective, EC prediction can be further conceptualized as a sequential regression problem akin to time series prediction, warranting the application of sequential deep learning methods. For sequential models, we denote F as the feature space and E as the target space. Here, $f_{i,j}^s \in F \subset \mathbb{R}^{N_s \times D_f}$ is an observed i-th feature of j-th trip at s-th segment, and $ec_{i,j} \in E \subset \mathbb{R}$ is the corresponding EC. Finally, the prediction model aims to learn parameters by minimizing the Mean Square Error (MSE) loss

$$\theta = argmin(loss_\theta^{reg}) = argmin \left(\frac{1}{j} \sum (e_j - M_{\theta(f)}))^2 \right) \tag{9}$$

where θ is the parameters to be learned and j is the number of trips. We have explored the performance of four different sequence deep learning approaches based on field data to select the best prediction model.

3.4.1. Long short-term memory and gate recurrent unit

Long Short-term Memory (LSTM) and Gated Recurrent Unit (GRU) emerge as frequently employed sequential prediction models, characterized by gating mechanisms designed for the comprehension of sequential data. The bidirectional structure further enhances the model's ability to extract inter-segment interdependencies. The structural diagram of an LSTM with a bidirectional structure is shown in Fig. 5.

The learning process of LSTM is expressed as Eq. (10). While this paper elucidates LSTM, the learning process of GRU can be cross-referenced in [8].

$$\begin{cases} \mathbf{i}_t = \sigma(\mathbf{W}_{x_t,i}\mathbf{X}_t + \mathbf{W}_{h_{t-1},i}\mathbf{H}_{t-1} + \mathbf{W}_{C_t,i}\mathbf{C}_{t-1} + \mathbf{b}_i) \\ \mathbf{f}_t = \sigma(\mathbf{W}_{x_t,f}\mathbf{X}_t + \mathbf{W}_{h_{t-1},f}\mathbf{H}_{t-1} + \mathbf{W}_{C_t,f}\mathbf{C}_{t-1} + \mathbf{b}_f) \\ \mathbf{c}_t = \mathbf{t}_t\mathbf{c}_{t-1} + \mathbf{i}_t \tan(\mathbf{W}_{x_t,o}\mathbf{X}_t + \mathbf{W}_{h_t,o}\mathbf{H}_{t-1} + \mathbf{b}_c) \\ \mathbf{o}_t = \sigma(\mathbf{W}_{x_t,o}\mathbf{X}_t + \mathbf{W}_{h_t,o}\mathbf{H}_{t-1} + \mathbf{W}_{C_t,o}\mathbf{C}_{t-1} + \mathbf{b}_o) \\ \mathbf{H}_t = \mathbf{o}_t \tan(\mathbf{C}_t) \end{cases} \tag{10}$$

where $\mathbf{i}_t,\mathbf{f}_t,\mathbf{c}_t,\mathbf{o}_t$ are the outputs of input gates i, forget gates f, output gates o and cell state c at time t, respectively. $\mathbf{W}_{x_t,i},\mathbf{W}_{x_t,f},\mathbf{W}_{x_t,o},\mathbf{W}_{x_t,c}$ are the weights of input $\mathbf{X}_t$ and input gates i, forget gates f, output gates o and cell state c, respectively. $\mathbf{W}_{h_t,i},\mathbf{W}_{h_t,f},\mathbf{W}_{h_t,o}$ are the weights of hidden layer output $\mathbf{H}_t$ and corresponding gated units. $\mathbf{W}_{c_t,i},\mathbf{W}_{c_t,f},\mathbf{W}_{c_t,o}$ are the weights of cell state output $\mathbf{C}_t$ and corresponding gated units. $\mathbf{b}_i,\mathbf{b}_f,\mathbf{b}_o,\mathbf{b}_c$ are the bias vectors, and σ is the activation function.

3.4.2. Temporal convolutional network

Temporal Convolutional Network (TCN) [3] represents a sequence model relying entirely on convolution. Unlike traditional convolutional neural networks, TCN operates without visibility into future data, adhering to strict temporal constraints. Empirical evidence attests to TCN's superiority over recurrent neural networks in specific sequence tasks

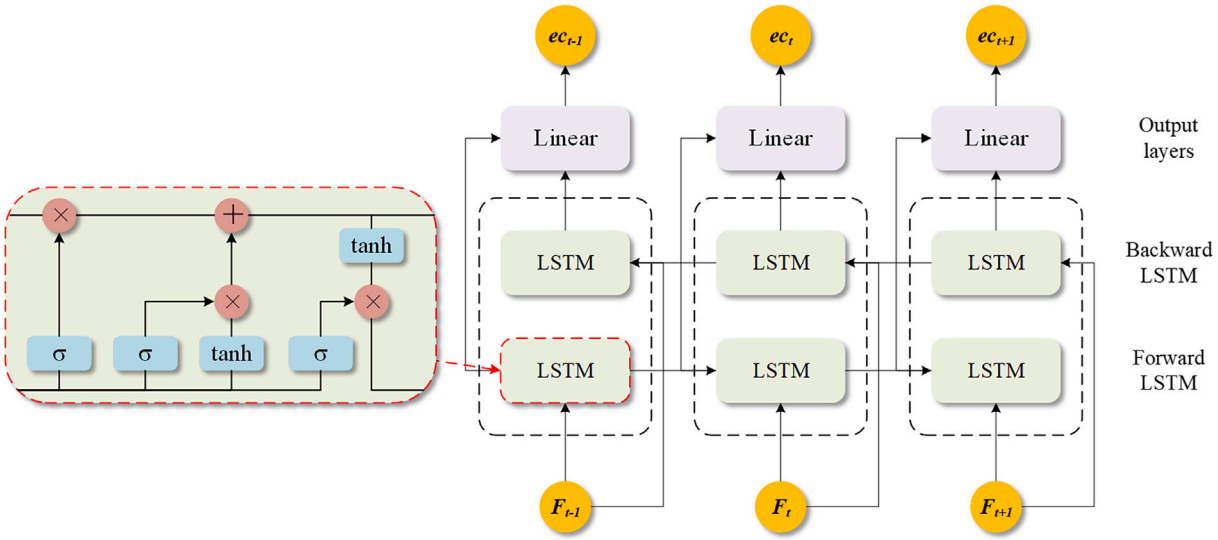

Fig. 5. LSTM structure with bidirectional learning.

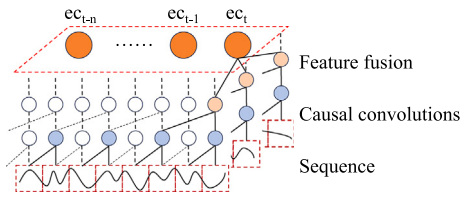

Fig. 6. The structure of TCN.

such as natural language processing and audio processing. The TCN structure is shown in Fig. 6.

Formally, for a sequential feature $F \subset \mathbb{R}^{N_s \times D_f}$ and a filter $\mathcal{F} \subset \mathbb{R}^k$, the temporal convolution with dilated factor is defined as,

$$\begin{cases} TC(F) = (F_{:,j} \otimes_d \mathcal{F})(f) = \sum_{s=1}^{N_s} \mathcal{F}_k F_{s-d \cdot i,j} \\ O_{res} = \sigma(F_{:,j} + TC(F_{:,j})) \end{cases} \tag{11}$$

where TC is the operation of temporal convolution, d is the dilation factor, k is the filter size and $s-d \cdot i$ is the index of the historical segment feature. O_{res} is the output of residual connections.

3.4.3. Transformer

The Transformer stands as the current state-of-the-art technology in natural language processing and long-term sequence prediction, employing a seq2seq framework for handling sequential inputs and outputs. Deploying positional encodings ensures that the attention mechanism captures the positional information of sequences. The structure of the Transformer is depicted in Fig. 7.

The learning process of the Transformer is defined as follows.

$$\begin{cases} Attention(Q,K,V) = softmax\left(\dfrac{QK^T}{\sqrt{d_k}}\right)V \\ MultiHead(Q,K,V) = Concat(head_1,\ldots,head_n)W^o \\ head_i = Attention(QW_i^Q, KW_i^K, VW_i^V) \end{cases} \tag{12}$$

where Q,K,V indicate the query, key, and value vectors, respectively. d_k is the scaling factor for a stable gradient, $W^O \in \mathbb{R}^{hd_v \times d_{model}}$,$W_i^Q \in \mathbb{R}^{d_{model} \times d_q}$, $W_i^K \in \mathbb{R}^{d_{model} \times d_k}$ and $W_i^V \in \mathbb{R}^{d_{model} \times d_v}$ are learnable weight matrices.

3.4.4. Model settings

The model training was conducted using Python 3.9 with the deep learning framework PyTorch version 1.12, and computations were performed on a computer equipped with an RTX 3070 Ti. This study initially

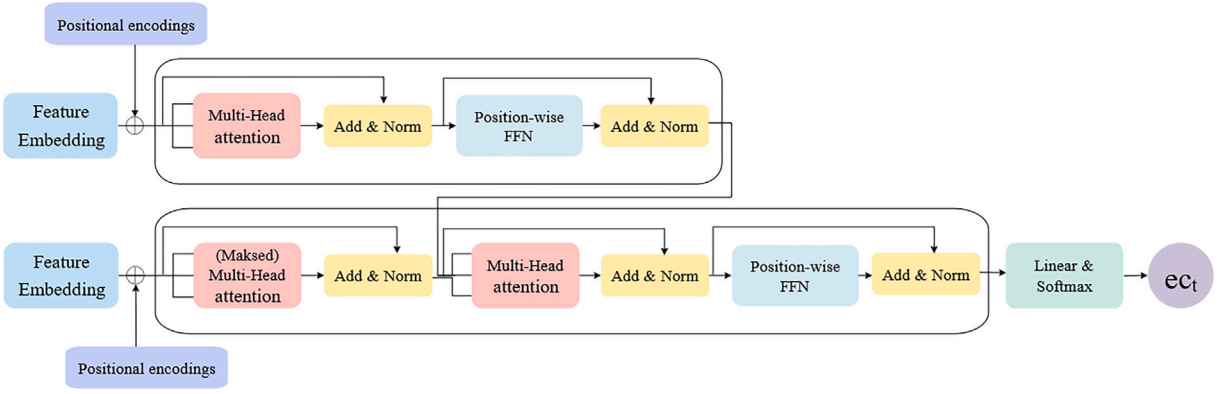

Fig. 7. The structure of Transformer.

Table 4
Hyperparameter settings for SA prediction.

	LSTM	GRU	TCN	Transformer
Hyper parameters	Structure [300,300]	Structure [64,64]	Structure [32,300]	Encoder structure [16,64]
			Kernel size 20	Decoded structure [64,16]
			Dilation factor 2	Number of heads 4
	Epoch 300	Epoch 500	Epoch 100	Epoch 100
	LR 0.0001	LR 0.0001	LR 0.0001	LR 0.0005
	dropout = 0.1	dropout = 0.1	dropout = 0.1	dropout = 0.5
Parameters	2.9 M	0.4 M	18.2 K	10.9 K

Table 5
The performance of SA and NSA prediction.

Prediction method	Model	SHEV dataset	SZEV dataset	CNEV dataset	Avg.
		MAE/RMSE/R^2	MAE/RMSE/R^2	MAE/RMSE/R^2	MAE/RMSE/R^2
NSA	SVM	3.14/3.34/0.91	3.118/3.224/0.9	2.989/3.12/0.92	3.082/3.228/0.91
	MLR	2.037/2.86/0.94	2.303/2.979/0.94	2.211/3.079/0.94	2.184/2.973/0.94
	DNN	2.268/3.262/0.91	2.225/2.944/0.95	1.955/2.722/0.96	2.149/2.976/0.94
	XGBoost	2.019/2.963/0.94	2.002/5.462/0.83	1.497/2.171/0.97	1.84/3.532/0.91
SA	Tnn	6.391/7.639/0.59	6.153/7.238/0.66	5.409/6.321/0.77	5.985/7.066/0.67
	TCN	1.389/1.901/0.97	1.991/2.639/0.95	1.675/2.439/0.97	1.685/2.326/0.96
	LSTM	0.915/1.327/0.99	1.719/2.31/0.96	0.915/1.327/0.99	1.183/1.654/0.98
	GRU	0.98/1.281/0.99	1.552/2.095/0.97	1.045/1.564/0.99	1.192/1.647/0.98

shuffled the trips in the datasets, and then divided each dataset into training, validation, and test sets in a ratio of 7:1:2. All models used the Adam optimizer and deployed the ReduceLROnPlateau technique to dynamically adjust the learning rate. When the model's loss on the validation set did not decrease for five consecutive epochs, the learning rate was reduced by 10 %. It is important to note that deep learning models are prone to overfitting when dealing with small datasets or noisy data. Therefore, we recommend using a dataset scale comparable to the current one for similar studies. If working with smaller datasets, it is advisable to consider simpler models and employ robust regularization techniques to mitigate overfitting risks. Additionally, careful data preprocessing and augmentation can help address the impact of noisy data on model performance. To ensure a fair comparison, this study searched for the best hyperparameter combinations of each model by grid search and compared the average prediction performance over three datasets. The hyperparameters for the SA prediction method are shown in Table 4. Computational complexity and scalability are common challenges for deep learning models. The parameters detailed in Table 4 elucidate the model complexity. Additionally, deploying the model in the cloud may address scalability concerns by optimizing computational efficiency through parallel computing and distributed training. In a cloud environment, users only need to upload data and receive results, which simplifies the computational burden for end-users. The hyperparameters for the ST prediction method are included in the appendix Table S2. To provide a comprehensive evaluation, we have included the Mean Absolute Error (MAE), Root Mean Square Error (RMSE), and R-Square (R^2) metrics. MAE offers an intuitive measure of average prediction error, while RMSE penalizes larger prediction errors. R^2 is a dimensionless metric that helps avoid potential biases due to differences in driving distances. The definitions can be mathematically expressed as:

$$\begin{cases} \mathrm{MAE} = \dfrac{1}{n}\sum_{i=1}^{n}\left|ec_i - \overline{ec_i}\right| \\ \mathrm{RMSE} = \sqrt{\dfrac{1}{n}\sum_{i=1}^{n}\left(ec_i - \overline{ec_i}\right)^2} \\ R^2 = \dfrac{\sum_{i=1}^{n}\left(ec_i - \overline{ec_i}\right)^2}{\sum_{i=1}^{n}\left(ec_i - \widehat{ec_i}\right)^2} \end{cases} \tag{13}$$

where ec_i, $\overline{ec_i}$, $\widehat{ec_i}$ are the real, predicted and average real energy consumption at i-th trip, respectively.

Meanwhile, this study chooses four representative non-sequential prediction models for EC prediction. These models have been widely adopted in recent studies on EC prediction for EVs, which are (1) Multivariate Linear Regression Model (MLR) [21], (2) Deep Neural Network (DNN) [2], (3) Support Vector Machine (SVM) [17], and (4) XGBoost [6]. These four models do not capture the sequence dependencies between segments and, therefore, serve as competing forecasting models against the methodology proposed in this study. Similarly, hyperparameters are determined through grid search. To balance effectiveness and computational cost, we designed search spaces grounded in prior studies and validated them through preliminary tests. Grid search was applied to a subset of sensitive hyperparameters, as summarized in Appendix Table S3.

4. Results

4.1. The comparison among prediction models

Table 5 provides a comparative evaluation between the NSA and SA prediction methods. The results indicate that the prediction accuracy of SA is higher than NSA (except Transformer), which emphasizes the importance of considering sequential dependencies among adjacent segments. XGBoost is the best model in the NSA prediction method, with an average MAE of 1.839 over the three datasets. In comparison, GRU is the best model in the SA prediction method, with an average MAE of 1.192, which is 35.1 % lower than that of XGBoost. This improvement can be attributed to the fact that SA-GRU treats segments akin to handling sequential data, considering the sequence interdependence between EC in segments. It is worth mentioning that Transformer performs poorly in the SA prediction approach, and is even lower than that of the NSA, hinting that Transformer model may not be a good candidate the for segment-accumulation EC prediction task herein.

Table 6 illustrates performance of NST and ST prediction methods. The results consistently emphasize that ST predictions generally surpass their NST counterparts. Models considering sequence interdependencies using sequential prediction provide 33 % higher accuracy on average. Among the ST prediction methods, GRU performs the best, with 35.2 % higher accuracy than Transformer. As for the NST prediction methods, XGBoost has the best performance, but its accuracy is 20.6 %

Table 6
The performance of ST and NST prediction.

Prediction method	Model	SHEV dataset	SZEV dataset	CNEV dataset	Avg.
		MAE/RMSE/R^2	MAE/RMSE/R^2	MAE/RMSE/R^2	MAE/RMSE/R^2
NST	SVM	3.169/3.711/0.9	2.721/3.32/0.93	2.648/3.261/0.94	2.846/3.431/0.92
	MLR	1.924/2.695/0.95	1.785/2.364/0.96	1.522/2.167/0.97	1.744/2.409/0.96
	DNN	1.93/2.638/0.95	1.977/2.572/0.96	2.024/2.678/0.96	1.977/2.629/0.96
	XGBoost	1.626/2.254/0.96	1.575/2.058/0.97	1.044/1.533/0.99	1.415/1.949/0.97
ST	Tnn	1.698/2.4/0.96	1.878/2.508/0.96	1.619/2.249/0.97	1.732/2.386/0.96
	TCN	1.104/1.609/0.99	1.583/2.135/0.97	1.125/1.636/0.98	1.271/1.793/0.98
	LSTM	1.033/1.421/0.99	1.623/2.198/0.97	1.016/1.436/0.99	1.224/1.685/0.98
	GRU	0.98/1.338/0.99	1.531/2.067/0.97	0.857/1.25/0.99	1.123/1.552/0.98

Table 7
The computational cost and efficiency of the proposed method.

Prediction method	SHEV dataset		SZEV dataset		CNEV dataset		avg. FLOPs
	Training	Inference	Training	Inference	Training	Inference	
SA-TNN	951.3	0.16	520.51	0.1	779.47	0.14	21.197 G
ST-TNN	938.1	0.14	513.29	0.08	768.65	0.12	
SA-TCN	354.2	0.5	193.8	0.25	290.22	0.4	1.211 T
ST-TCN	423	0.55	231.45	0.3	346.59	0.45	
SA-LSTM	1905.23	0.25	1042.46	0.15	1561.09	0.2	151.284 G
ST-LSTM	1373.58	0.2	751.57	0.1	1125.47	0.15	
SA-GRU	2061.3	0.4	1127.86	0.2	1688.96	0.35	113.771 G
ST-GRU	2267.45	0.3	1240.66	0.15	1857.88	0.25	

Note: the unit of training and inference time is seconds.

Table 8
The MAE of conventional and proposed methods.

Prediction method	Model	SHEV dataset	SZEV dataset	CNEV dataset	Avg.
		MAE/RMSE/R^2	MAE/RMSE/R^2	MAE/RMSE/R^2	MAE/RMSE/R^2
Conventional methods	ECR*DIST	6.268/7.708/0.58	4.42/5.564/0.8	2.197/3.376/0.93	4.295/5.549/0.77
	MLR	2.002/2.803/0.94	2.198/2.859/0.95	2.793/3.553/0.92	2.331/3.072/0.94
Proposed methods	SA-LSTM	0.915/1.327/0.99	1.719/2.31/0.96	0.915/1.327/0.99	1.183/1.654/0.98
	ST-GRU	0.98/1.338/0.99	1.531/2.067/0.97	0.857/1.25/0.99	1.123/1.552/0.98

lower than that of GRU. This may be attributed to the inherent limitations of non-sequential models disregarding potential accuracy gains provided by sequence-dependent effects of adjacent segments on EC of a trip. In a similar context, the performance of TCN surpasses that of XGBoost, with prediction errors being 7.2 % lower. It is interesting that in the sequential trip-level prediction context, Transformer presents superior performance compared to NST models (except XGBoost), which is different from the performance of SA and NSA models in Table 5.

Comparing the prediction methods of SA and ST (see Tables 5 and 6), on average, the prediction performance of ST is superior to SA. However, the results indicate that the methods of SA and ST have pros and cons, depending on the datasets. Taking LSTM as an example, the MAE of SA-LSTM is 0.118 and 0.108 lower than that of ST-LSTM on both SHEV and CNEV datasets, but it is 0.096 higher than that of ST-LSTM on the SZEV dataset. However, the overall perspective does not disclose significant differences. Therefore, the selection of a superior solution should be contingent on local data.

To ensure the practical feasibility of our method in real-time, in-vehicle deployment scenarios, we conducted a thorough evaluation of its computational efficiency. As summarized in Table 7, all models complete training within 40 minutes, which implies low retraining cost—beneficial for transfer learning applications or adaptation to distributional drift over time. In terms of inference performance, even the most computationally intensive model (Transformer) requires only 0.28 s for the entire test set (i.e., less than 0.21 milliseconds per trip on average), confirming that our models meet the low-latency requirements of real-time energy consumption prediction. All experiments were conducted on an NVIDIA RTX 3070 Ti GPU. Given that predictions are typically generated once per trip during pre-departure planning, this level of latency is well within acceptable limits even for onboard CPU-based systems or embedded platforms. These results collectively confirm that our models are not only accurate but also computationally efficient and deployment-ready for real-time applications in energy-aware intelligent vehicles.

4.2. The comparison to conventional methods and residual analysis

In this study, two widely-used conventional methods of trip energy prediction serve as competing forecasting models to demonstrate the effectiveness of the proposed methods. (1) ECR×dist: This method involves multiplying the Energy Consumption Rate (ECR, measured in kWh/100 km) provided by the manufacturer by the expected distance of the trip. (2) Multiple Linear Regression (MLR): This method utilizes the expected distance, average speed, and temperature as independent variables to predict energy consumption. The results are shown in Table 8.

The findings reveal a notable MAE when predicting trip energy consumption using the manufacturer-provided ECR, which can be ascribed to its derivation from testing conducted in ideal operating environments. Real-world driving conditions are inherently more intricate, often leading to actual ECR surpassing those provided by the manufacturer. Additionally, MLR yields suboptimal outcomes due to its incapacity to capture the intricate relationship between the independent variables and

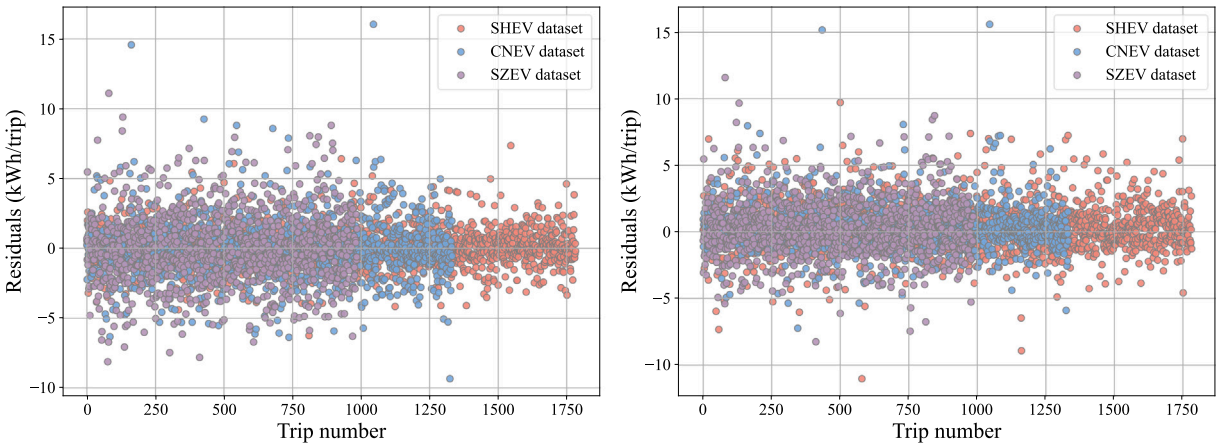

Fig. 8. Residual analysis of the proposed model.

Table 9
Uncertainty quantification of proposed methods.

Prediction method	Model	SHEV dataset		SZEV dataset		CNEV dataset		Avg.	
		PICP	MPIW	PICP	MPIW	PICP	MPIW	PICP	MPIW
SA	Tnn	–	–	–	–	–	–	–	–
	TCN	89.7 %	6.03	82.2 %	6.16	89.0 %	6.15	87.0 %	6.11
	LSTM	96.1 %	6.15	79.7 %	6.16	89.8 %	6.17	88.6 %	6.16
	GRU	94.2 %	6.05	84.4 %	6.21	91.3 %	6.23	90.0 %	6.17
ST	Tnn	21.6 %	7.95	16.9 %	8.38	19.4 %	8.39	19.3 %	8.24
	TCN	90.9 %	6.15	88.6 %	6.24	95.3 %	6.28	91.6 %	6.22
	LSTM	91.2 %	6.21	80.4 %	6.04	85.8 %	5.92	85.8 %	6.06
	GRU	92.3 %	6.01	88.0 %	6.29	94.5 %	6.30	91.6 %	6.20

Note: indicates results lacking practical significance.

EC. Moreover, MLR disregards sequence interdependencies among adjacent segments, thereby diminishing prediction accuracy. A comparative analysis of the average MAE across the three datasets underscores a substantial enhancement of 65.2 % in prediction accuracy with the proposed methods compared to the conventional methods.

This study investigates discrepancies between predicted and actual energy consumption. Fig. 8 illustrates the residual distributions of two representative models. The residuals of SA-LSTM are relatively evenly distributed around zero, whereas ST-GRU exhibits higher residuals. The tendency of ST-GRU to underestimate actual values is particularly concerning as it may lead to overly optimistic estimates of remaining driving distances for drivers. Consequently, the SA method is recommended. Additionally, we observe significant divergences between model predictions and actual values across different trips. This variation suggests that different models prioritize trip-specific pattern learning differently, despite using identical datasets. Interpreting deep learning model predictions remains a persistent challenge.

4.3. Uncertainty quantification and robustness evaluation

Compared to point estimates, probabilistic prediction intervals offer more informative guidance, which is especially beneficial for practical decision-making by EV drivers. To quantify uncertainty, we adopt Monte Carlo dropout [13]—a widely used Bayesian approximation technique that generates multiple stochastic predictions by randomly deactivating neurons during inference. Specifically, we perform 100 stochastic forward passes to approximate the predictive distribution, which enables the construction of 95 % confidence intervals for each prediction. The quality of uncertainty estimation is evaluated using two standard metrics: Prediction Interval Coverage Probability (PICP) and Mean Prediction Interval Width (MPIW).

As shown in Table 9, most models achieve PICP values above 85 %, indicating high reliability of the generated intervals. In particular, ST-GRU and ST-TCN consistently deliver both high coverage and narrow interval widths, demonstrating a favorable trade-off between confidence and informativeness. In contrast, the TNN baseline under the SA setting fails to produce meaningful interval estimates, and under the ST setting, it yields insufficient coverage, highlighting its limitations in uncertainty-aware predictions. Overall, ST-based methods outperform SA-based methods in terms of uncertainty quantification. This advantage may stem from the sequential aggregation nature of SA, where prediction uncertainty accumulates across multiple segments, thereby amplifying total variance. In contrast, ST-based approaches estimate trip-level energy consumption directly, thus avoiding compounded uncertainty. Based on these findings, we recommend ST-based methods for providing probabilistic energy consumption prediction in real-world EV applications.

We further visualize the prediction intervals using SA-LSTM and ST-GRU as representative models. For clarity, we selected 50 driving trips across the three datasets. As shown in Fig. 9, the vast majority of ground truth values lie within the corresponding 95 % confidence intervals, reinforcing the reliability of the predictive distributions. These probabilistic predictions can help inform decisions related to charging, routing, or eco-driving strategies—ultimately supporting more confident and informed driving behavior under uncertainty.

To evaluate robustness, we conducted additional experiments by injecting additive Gaussian noise into the input features, with standard

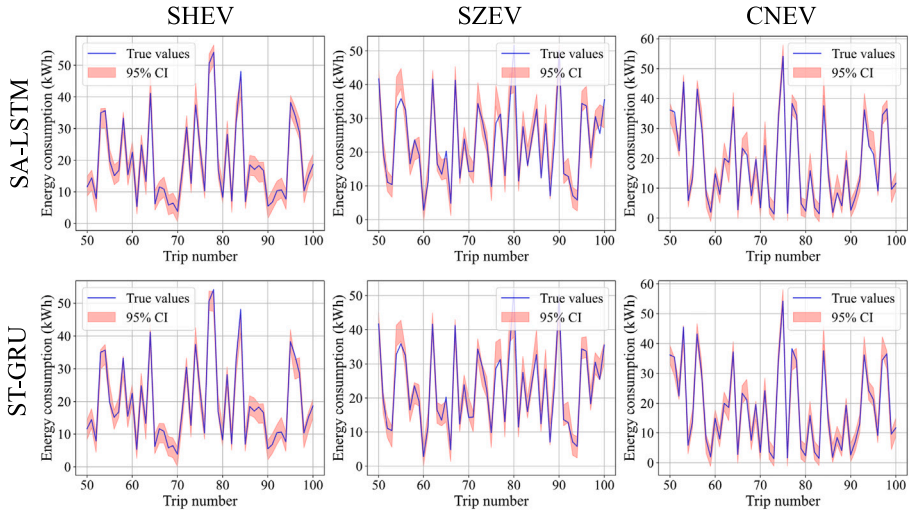

Fig. 9. Samples on uncertainty quantification across multiple datasets.

Table 10
Robustness validation of proposed methods.

Prediction method	Noise Std	SHEV dataset			CNEV dataset			SZEV dataset		
		MAE	RMSE	R^2	MAE	RMSE	R^2	MAE	RMSE	R^2
SA-LSTM	0.03	1.152	1.656	0.98	1.745	2.342	0.96	1.036	1.413	0.99
	0.06	1.673	2.364	0.94	1.814	2.404	0.96	1.358	1.758	0.98
	0.09	2.177	3.05	0.9	1.871	2.466	0.96	1.658	2.074	0.97
	0.12	2.895	3.965	0.81	2.024	2.65	0.95	2.119	2.566	0.95
	0.15	3.297	4.556	0.75	2.169	2.783	0.95	2.558	3.105	0.92
ST-GRU	0.03	1.257	1.713	0.98	1.534	2.072	0.97	0.951	1.335	0.99
	0.06	1.773	2.328	0.95	1.596	2.127	0.97	1.263	1.659	0.98
	0.09	2.338	3.068	0.9	1.664	2.206	0.97	1.63	2.011	0.96
	0.12	2.932	3.847	0.83	1.8	2.375	0.96	1.949	2.416	0.95
	0.15	3.435	4.452	0.77	1.902	2.493	0.96	2.377	2.893	0.92

deviations ranging from 0.03 to 0.15. Table 10 summarizes the resulting changes in prediction performance across three datasets using MAE, RMSE, and R^2 metrics. Despite the increased noise levels, both SA-LSTM and ST-GRU models maintain high R^2 values (≥ 0.95) under moderate noise ($\sigma \leq 0.09$), and only experience gradual degradation at higher noise levels. Notably, ST-GRU demonstrates superior resilience, with R^2 remaining at 0.96 even at $\sigma = 0.12$ in most scenarios. These results confirm that our models are not only accurate under ideal conditions but also robust to input perturbations—supporting their deployment in real-world, noisy environments.

4.4. Influencing factors of EC

There is a clarification that should be explained before the analysis. In this study, the object of analysis is the segment, not the trip, and each segment has a standard length of 1 km. Therefore, the energy consumption (kWh) for each segment is equivalent to the Energy Consumption Rate (ECR, kWh/km).

4.4.1. Driving speed and ECR

Fig. 10 visually illustrates discrepancies in ECR across different ranges of speed. The left y-axis represents the box plots of the distribution of ECR at different speed ranges. The right y-axis and red dashed line represent the average ECR under the corresponding speed range with a different scale. The results show a consistent pattern across the three datasets where the ECR initially decreases and then increases with speed, aligning with prior research findings [11]. This phenomenon can be attributed to the fact that low-speed driving in urban contexts generally involves frequent acceleration and deceleration, whereas higher speeds lead to a significant increase in air resistance, resulting in a higher ECR. For SHEV and SZEV, the EVs achieve their lowest ECR at the speed ranging from 70 to 80 km/h, while CNEV's EVs reach their minimum ECR at the speed between 50 and 60 km/h. Differences in the optimal speed observed across different datasets result from the combined effects of distinct vehicle models and traffic conditions in different cities. It is noteworthy that, in all three datasets, the current operating speeds of EVs primarily fall within the 10–20 km/h range (the second box), constituting 23.5 %, 20.5 %, and 14.6 %, respectively. The speed range is significantly lower than the mentioned optimal speed range. If these EVs operated at optimal speeds, potential energy savings could amount to 6.63, 3.59, and 3.46 kWh per 100 km on average for the vehicles in the datasets of SHEV, SZEV, and CNEV, respectively. These findings collectively emphasize the critical importance of speed on energy efficiency.

4.4.2. Temperature and ECR

Fig. 11 shows the impacts of temperature on ECR. Specifically, the results from SHEV manifest the lowest average ECR within the temperature range of 15–20 °C, whereas the results from SZEV and CNEV demonstrate the lowest average at temperatures of 20–25 °C. These results are corroborated by prior research that indicates the optimal temperature of 18 °C [49]. The pattern may be attributed to drivers commonly activating air conditioning in both low and high temperatures, substantially escalating EC. Relative to the optimum temperature, average ECR elevates by 6.5 % and 8.4 % in the lowest and highest

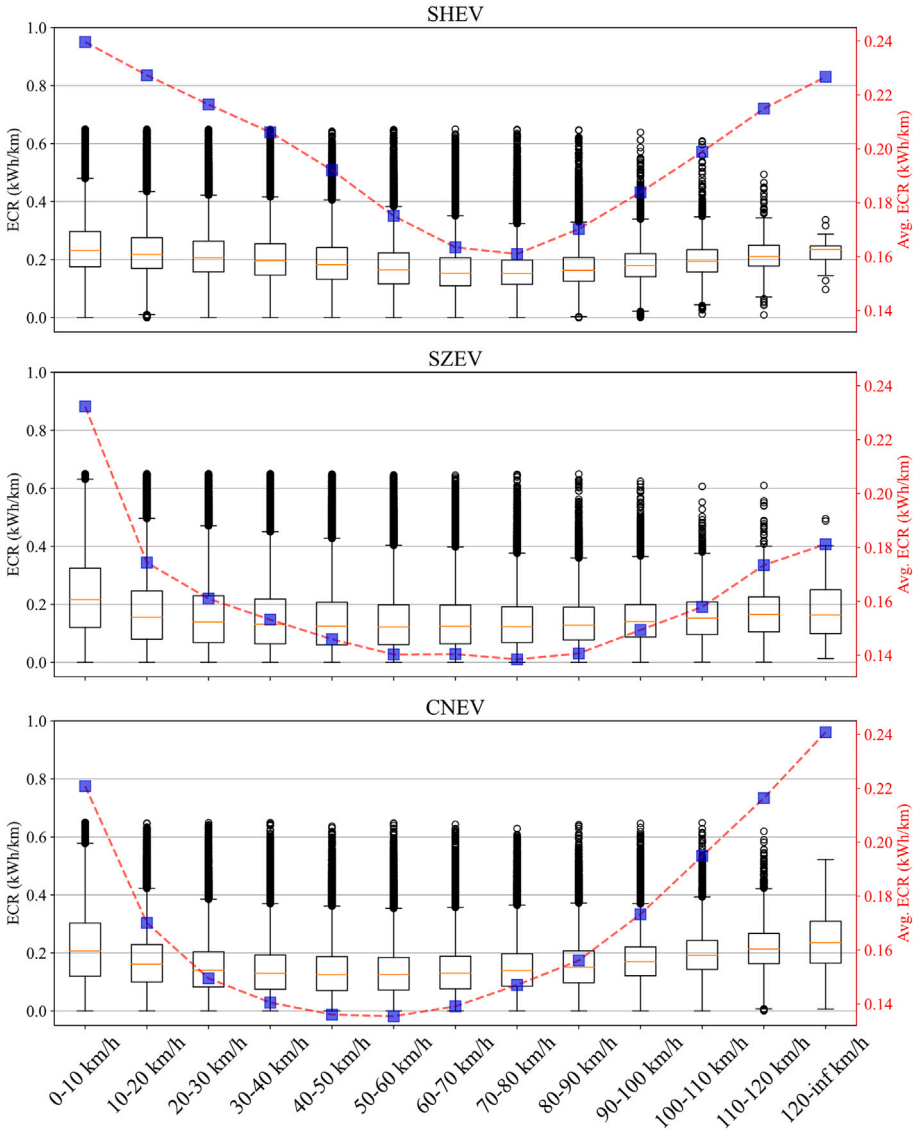

Fig. 10. Relationship between speed and ECR (The left y-axis is the ECR, and the right y-axis is the average ECR with different scales).

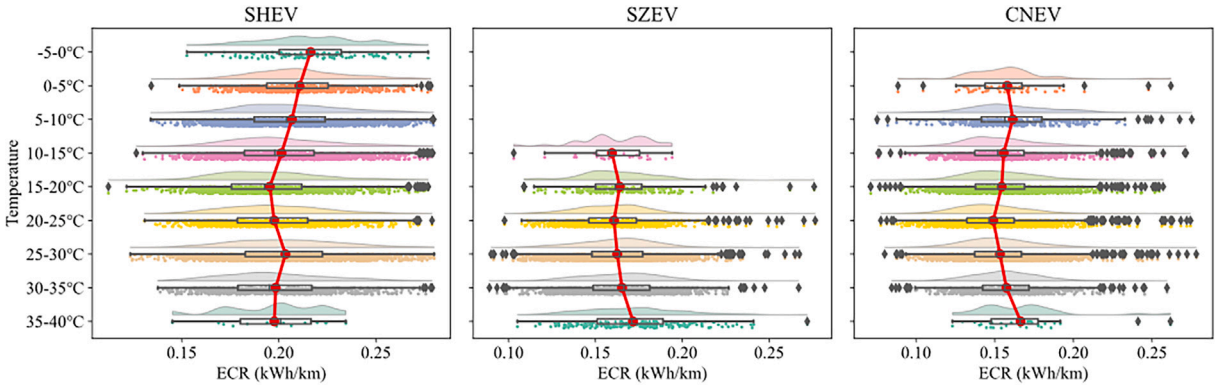

Fig. 11. Relationship between temperature and ECR.

temperature ranges, respectively. Variances across cities are notable. In Shanghai, low temperatures significantly augment ECR. In contrast, in Shenzhen and six other cities, high temperatures exert a more substantial impact on increasing ECR. This divergence may arise from climate differences among cities, influencing factors such as drivers' air conditioning usage habits and driving behavior.

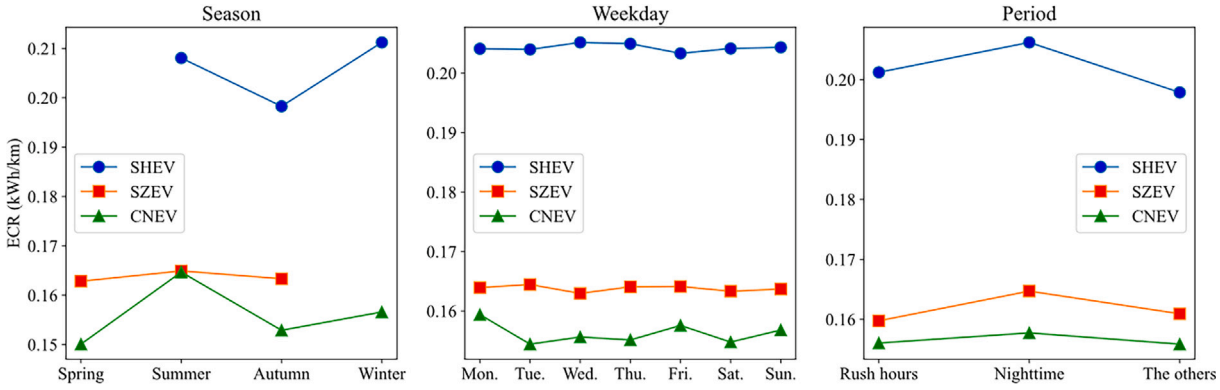

Fig. 12. Relationship between time-related features and ECR.

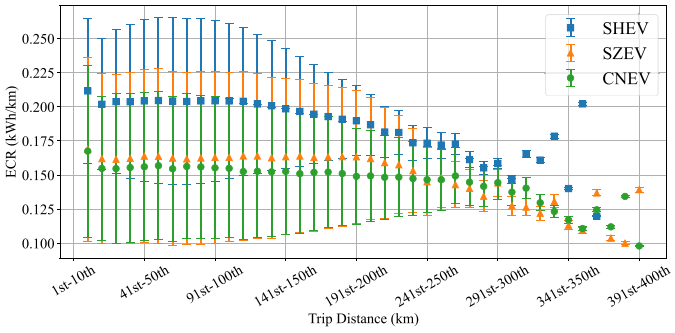

Fig. 13. ECR for different trip distance.

4.4.3. Time-related features and ECR

Fig. 12 delves into the variations in ECR concerning different time-related features. The results of seasonal features indicate that ECR is lower during spring and autumn compared to summer and winter. This distinction may be primarily attributed to increased air conditioning usage in summer and winter, resulting in elevated ECR. Specifically, ECR in summer and winter exhibits a 4.1 % increase relative to spring and autumn. Additionally, rush hours demonstrate negligible impact on ECR. Conversely, ECR notably increases during nighttime driving. This may be predominantly due to increased headlight usage and higher speeds during the night, leading to high EC. In comparison to other periods, nighttime trips demonstrate a 2.1 %–2.5 % increment in ECR on average. Lastly, the day of the week exerts minimal influence on ECR, implying that trips on different working days do not show significant differences in ECR.

4.4.4. Relation of driving distance and depth of discharge with ECR

In this study, a trip is divided into continuous and ordered segments of 1 km. Fig. 13 shows how ECR changes as the driving distance increases. The outcomes underscore that as driving distance increases, the average ECR is pretty stable at the beginning and decreases after around 200 km. A common finding is that there are substantial variations, implying a lot of other factors affecting the ECR. The ECR of driving range 1st-10th km, is the highest. As the trip extends to 291st-300th km, the ECR stabilizes at a low point, marking about a 20 % decrease compared to the ECR in the range of 1st-10th km. The results from SHEV exhibit a different trend in ECR compared to the other two datasets for distances exceeding 300 km. This disparity may be attributed to the low sample size and some extreme values of SHEV data in the range exceeding 300 km.

Fig. 14 provides the relationship between DOD and ECR. The results demonstrate that when DOD was at 20–80 %, ECR shows a stable plateau pattern. Nevertheless, if the DOD falls exceeds 80 %, the ECR experiences a rapid reduction. Driving distance directly influences changes in DOD, and ECR typically decreases as distance increases, as depicted in Fig. 13, which is consistent with the decrease in ECR with increasing DOD. Therefore, a careful decoupling of the influences of other factors is necessary when analyzing the relationship between DOD and ECR. Although DOD is commonly used as an indicator, it is a processed metric provided by the Battery Management System (BMS) and may not fully encapsulate the actual energy use of the vehicle. This means that a 1 % increase in DOD at different initial DODs may correspond to different amounts of real EC.

4.5. Model interpretation

This study examines whether the predicted EC from trained prediction models aligns with real-world patterns, which tries to validate the

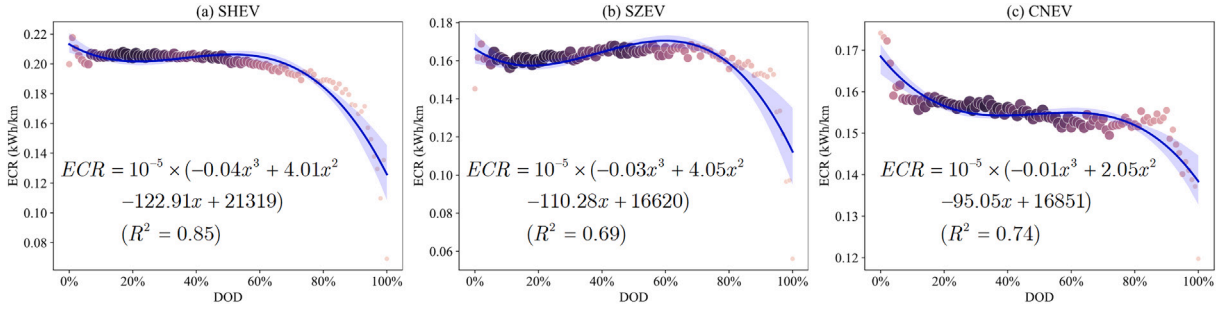

Fig. 14. Relationship between DOD and ECR.

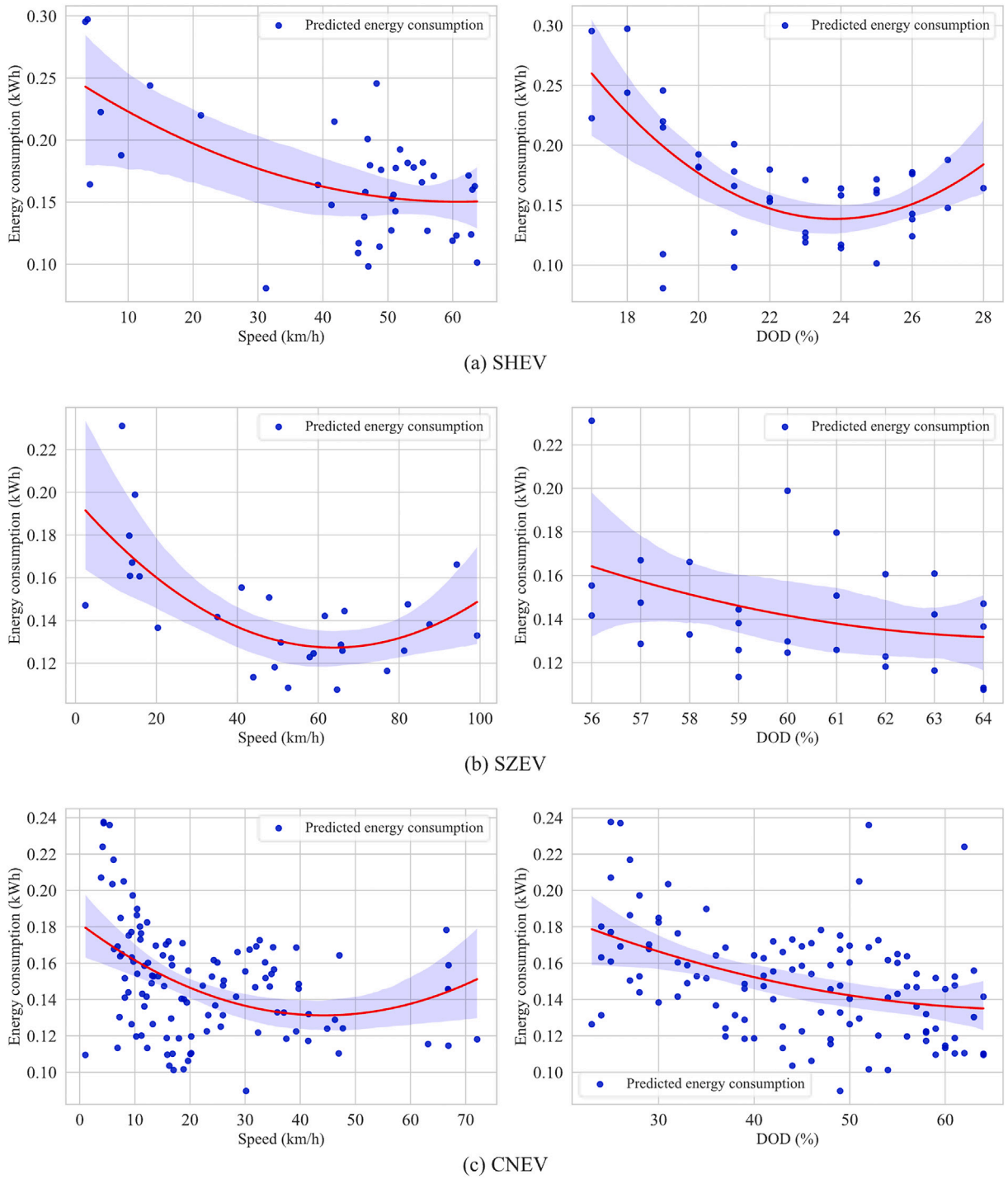

Fig. 15. Influence of speed and DOD on predicted energy consumption.

reliability of our proposed prediction models. Taking SA-GRU as an illustrative case (given that SA models offer predictions for each segment), three trips with several segments of 1 km are randomly chosen from each dataset, and the relationship between predicted EC and speed/DOD is depicted in Fig. 15.

For the speed-EC relationship, predicted EC follows a decreasing-then-increasing trend, aligning with real-world patterns, comparing Fig. 10. Regarding the DOD-EC relationship, predicted EC reaches a minimum at approximately 20 % DOD, exhibiting an overall decreasing trend within the 30–60 % DOD range, in line with actual observations, comparing Fig. 14. These outcomes emphasize that the SA method yields credible predictions and can effectively capture the interdependence between predicted EC and influencing factors. It is important to note that the wide dispersion of data points results from selecting several case trips. The high degree of uncertainty in individual trips makes it challenging to align closely with statistical trends. Capturing the uncertainties inherent in trips is crucial for enhancing the interpretability.

Fig. 16 delves into the impact of trip distance on the prediction accuracy of sequential predictions. The trips are categorized into six groups based on trip distance. The results indicate that the model

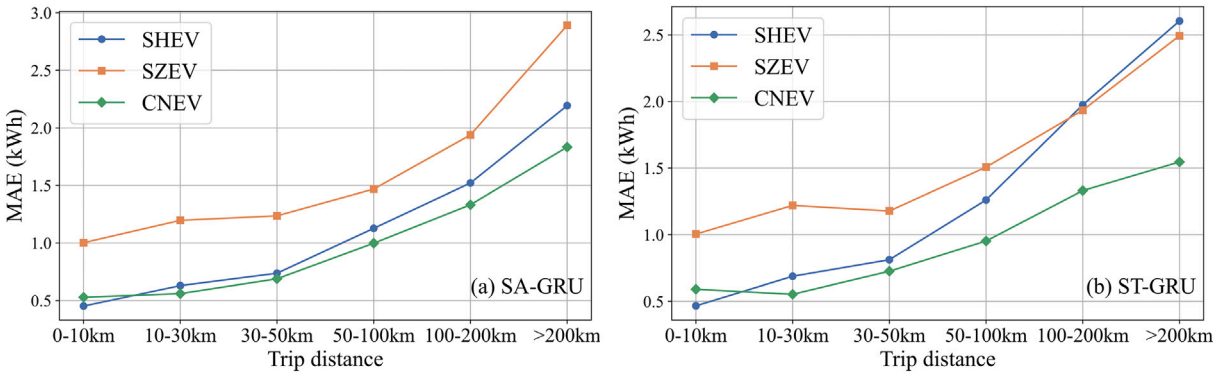

Fig. 16. Prediction errors for different travel distances.

exhibits a higher prediction error for longer trips, likely due to increased uncertainty associated with longer distances. The average MAE across three datasets reveals that, in the case of SA-GRU, predicting EC during trips exceeding 200 km results in a 68.9 % higher MAE compared to predicting EC for trips within the 0–10 km range. In the context of ST-GRU, the related MAE for predicting EC during trips exceeding 200 km is 71.3 % higher than that for trips within the 0–10 km range.

5. Discussion

This study presents a sequence-aware EC prediction framework using pre-trip accessible data. The reasoning for considering sequential dependencies in energy consumption lies in the assumption that adjacent road segments share energy consumption information, which facilitates forecasting compared to predicting each segment separately. Specifically, EVs travel through segments sequentially over time. The features and energy consumption of consecutive road segments may be likened to a time series. Past and neighboring data points of energy consumption provide useful information for enhancing the prediction accuracy of the current energy consumption by capturing similarities among adjacent road segments. Similarly, the study proposes that the average speed, duration, other features, and energy consumption from adjacent segments could be helpful in predicting the energy consumption of the current road segment. For instance, a vehicle accelerating in one segment will likely affect its energy consumption in subsequent segments due to the inertia and momentum carried over. There are also similarities in speed profiles, road slopes, and auxiliary usage of EVs in adjacent road segments. This sequential dependency leverages patterns and information embedded in the sequence of segments.

Despite promising results, several limitations should be acknowledged. First, we acknowledge that the black-box nature of deep learning models presents challenges for interpreting how input features contribute to prediction outcomes. While our study emphasizes predictive performance, we recognize the importance of model transparency in safety-critical and decision–support applications. Recent work has proposed interpretable hybrid architectures, such as attention-augmented variational autoencoders with adversarial regularization [27], which disentangle latent representations and highlight salient temporal features. Although our current framework does not implement such components, we view this as a promising direction. Future extensions could incorporate attention-based disentanglement or generative backbones to enhance interpretability and uncover causal patterns in energy consumption across sequential driving segments.

Second, identifying key predictors and their interactions is essential for understanding energy efficiency. However, common explainability tools are tailored for 2D input formats and are not directly applicable to the 3D sequence inputs used in this study. Moreover, multicollinearity among features may impair the reliability of such attribution scores. Future extensions may benefit from domain-informed disentanglement techniques or interpretable sequence-specific models.

Lastly, the ability of different models to capture long-range dependencies is an important consideration. Although LSTM and GRU mitigate gradient issues via gating mechanisms, they still suffer from limited memory capacity, leading to degraded performance on longer trips. In contrast, Transformers offer theoretical advantages through global self-attention but perform poorly in our case. This may be due to the relatively short average sequence length, the limited dataset size, and the structured, low-dimensional nature of our inputs, which reduces the effectiveness of attention mechanisms. These findings align with previous work [34] and highlight the need for tailored architectures—such as memory-augmented or hybrid models—for long-sequence energy prediction tasks.

Despite the aforementioned limitations, our framework offers significant real-world value. By enabling pre-trip EC predictions without requiring future speed profiles, it facilitates range-aware route planning for EV drivers, supports eco-driving behavior, and aids fleet operators in energy forecasting. The approach is lightweight and relies solely on data available before trip initiation, making it suitable for integration into onboard navigation systems, fleet management dashboards, or energy-aware trip planning mobile apps.

6. Conclusions

This study endeavors to propose a sequence-aware deep learning methodology for energy consumption prediction of electric vehicles. It discretizes trips into segments and conceptualizes EC prediction as a sequential task, considering sequence interdependencies among adjacent segments. All inputs are sourced from pre-trip obtainable data rather than unrealistic assumptions that presuppose access to future speed profiles per second throughout a trip. The main findings are as follows.

Embedding awareness of sequential dependence is advantageous for enhancing the accuracy of energy consumption prediction. Compared to traditional methods of treating the trip as a single entity, discretizing the trip into segments and sequentially capturing interdependencies within adjacent segments of energy consumption using deep learning methodology provides notable gains in prediction accuracy and interpretative ability. It is important to emphasize that the inputs required for our proposed methodologies are based on pre-trip and practically attainable data, not unrealistic high-resolution data. It offers new insights into methodologies for modeling more accurate and reliable energy consumption predictions for practical usage.

This study investigates the impact of factors on energy consumption from a segment-level perspective. The results show that: (1) The ECR gradually decreases during the trip, with the initial segment exhibiting the highest energy consumption rate, approximately 20 % higher than that of the segment just before the trip concludes; (2) The average ECR in

both summer and winter is 4.1 % higher than that in spring and autumn and higher ECR (2.1–2.5 %) is observed in nighttime driving compared to the rush hour and other times. (3) The relationship between ECR and both the speed within the segment and the depth of discharge can be clearly identified.

CRediT authorship contribution statement

Haichao Huang: Writing – review & editing, Writing – original draft, Visualization, Software, Methodology, Investigation, Formal analysis, Data curation, Conceptualization. **Kun Gao:** Writing – original draft, Supervision, Methodology, Formal analysis, Conceptualization. **Yizhou Wang:** Writing – review & editing. **Arsalan Najafi:** Writing – review & editing. **Zhe Zhang:** Conceptualization. **Hongdi He:** Writing – review & editing, Supervision, Formal analysis.

Code and data availability

The code and data used to reproduce the results presented in this paper are available at the following repository: https://www.github.com/RaganrokV/Sequential_EC_prediction. The EV data are available from Chinese government but restrictions apply to the availability of these data, which were used under license for the current study, and so are not publicly available.

Declaration of competing interest

The authors declare that they have no known competing financial interests or personal relationships that could have appeared to influence the work reported in this paper.

Acknowledgments

This work was supported by the National Natural Science Foundation of China (No.12072195), JPI Urban Europe, Energimyndigheten (e-MATS, P2023-00029) and Area of Advance Transport at Chalmers University of Technology. Haichao Huang acknowledges a scholarship from the China Scholarship Council (CSC) (202406230213).

Appendix

See Tables S1–S3 and Fig. S1.

Table S1
Dataset sample.

Field	Sample1	Sample2	Sample3
collectiontime	2021–07-31 09:53:20	2021–07-31 09:53:30	2021–07-31 09:53:40
vehicledata_vehiclestatus	1	1	1
vehicledata_chargestatus	3	3	3
vehicledata_runmodel	1	1	1
vehicledata_speed	0	0	0
vehicledata_summileage	71352	71352	71352
vehicledata_sumvoltage	395	395	394.8
vehicledata_sumcurrent	0.5	2.8	3.4
vehicledata_soc	99	99	99
vehicledata_dcdcstatus	1	1	1
vehicledata_gearnum	15	15	15
vehicledata_insulationresistance	4886	4616	4587
extremevalue_maxvoltagebatterysubseq	1	1	1
extremevalue_maxvoltagebatterysingleseq	96	96	96
extremevalue_maxbatterysinglevoltageval	4.131	4.131	4.13
extremevalue_minvoltagebatterysubseq	1	1	1
extremevalue_minvoltagebatterysingleseq	5	5	5
extremevalue_minbatterysinglevoltageval	4.108	4.108	4.106
extremevalue_maxtmpsubseq	1	1	1
extremevalue_maxtmpprobesingleseq	8	2	2
extremevalue_maxtmpval	31	31	31
extremevalue_mintmpsubseq	1	1	1
extremevalue_mintmpprobesingleseq	1	1	1
extremevalue_mintmpval	30	30	30
chargedevicevoltagelist_chargedevicevoltagenum	1	1	1
chargedevicevoltagelist_voltagelist_rechargeablestoragesubseq	[1]	[1]	[1]
chargedevicevoltagelist_voltagelist_rechargeablestoragevoltage	[395.0]	[395.0]	[394.8]
chargedevicevoltagelist_voltagelist_rechargeablestorageelectric	[0.5]	[2.8]	[3.4]
chargedevicevoltagelist_voltagelist_sumbatterysingle	[96]	[96]	[96]
chargedevicevoltagelist_voltagelist_firstbatteryseq	[1]	[1]	[1]
chargedevicevoltagelist_voltagelist_sumsinglebattery	[96]	[96]	[96]
chargedevicetemplist_chargedevicetempnum	1	1	1
chargedevicetemplist_templist_rechargeablestoragesubseq	[1]	[1]	[1]
chargedevicetemplist_templist_rechargeablestoragetmpnumber	[24]	[24]	[24]

Table S2
Hyperparameter settings for ST prediction.

	LSTM	GRU	TCN	Transformer
Hyper parameters	Structure [300,300]	Structure [256,256]	Structure [300,300] Kernel size 20 Dilation factor 2	Encoder structure [16,64] Decoded structure [64,16] Number of heads 4
	Epoch 300 LR 0.0001 dropout = 0.1	Epoch 500 LR 0.0001 dropout = 0.1	Epoch 100 LR 0.0001 dropout = 0.1	Epoch 100 LR 0.0005 dropout = 0.5
Parameters	2.9 M	1.5 M	0.2 M	10.9 K

Table S3
Search ranges for each model.

Model	Hyperparameter	Search Range
TNN	LR	0.001,0.0005,0.0001
	Heads	2,4
	Dropout	0.3,0.5
TCN	Hidden size	32,128,256,300
	Kernel size	10,20
LSTM	Hidden size	32,128,256,300
	Layers	1,2
GRU	Hidden size	32,128,256,300
	Layers	1,2
XGB	LR	0.1,0.05
	n_estimators	100,200,300
SVR	Kernel	RBF, Linear
	C	1,5,10
DNN	LR	0.001,0.0001
	Hidden size	64,128,256

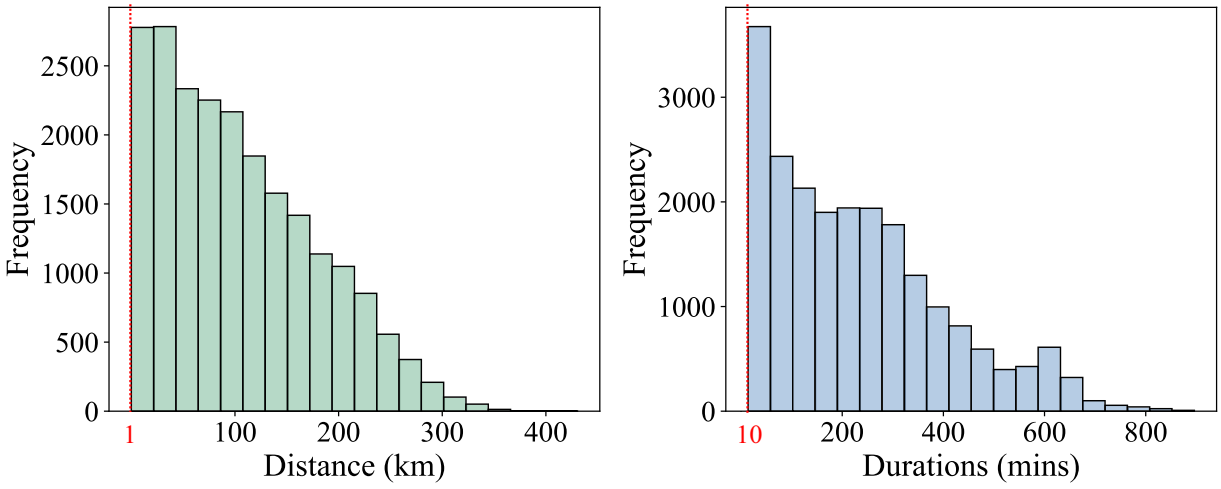

Fig. S1. Histogram of distances and durations after trip division.

Data availability

The authors do not have permission to share data.

References

[1] Abdelaty H, Al-Obaidi A, Mohamed M, Farag HE. Machine learning prediction models for battery-electric bus energy consumption in transit. Transp Res Part D Transp Environ 2021;96:102868. https://doi.org/10.1016/j.trd.2021.102868. https://linkinghub.elsevier.com/retrieve/pii/S1361920921001693

[2] Adedeji BP. Electric vehicles survey and a multifunctional artificial neural network for predicting energy consumption in all-electric vehicles. Results Eng 2023;19:101283. https://doi.org/10.1016/j.rineng.2023.101283. https://linkinghub.elsevier.com/retrieve/pii/S2590123023004103

[3] Bai S, Kolter JZ, Koltun V. An empirical evaluation of generic convolutional and recurrent networks for sequence modeling. 2018. http://arxiv.org/abs/1803.01271. arXiv:1803.01271 [cs].

[4] Basso R, Kulcsár B, Egardt B, Lindroth P, Sanchez-Diaz I. Energy consumption estimation integrated into the electric vehicle routing problem. Transp Res Part D Transp Environ 2019;69:141–67. https://doi.org/10.1016/j.trd.2019.01.006. https://linkinghub.elsevier.com/retrieve/pii/S1361920918304760

[5] Bi J, Wang Y, Sai Q, Ding C. Estimating remaining driving range of battery electric vehicles based on real-world data: a case study of Beijing, China. Energy 2019;169:833–43. https://doi.org/10.1016/j.energy.2018.12.061. https://linkinghub.elsevier.com/retrieve/pii/S0360544218324277

[6] Chen X, Lei Z, Ukkusuri SV. Prediction of road-level energy consumption of battery electric vehicles. In: 2022 IEEE 25Th International Conference on Intelligent Transportation Systems (ITSC); Macau, China: IEEE; 2022. p. 2550–5. https://doi.org/10.1109/ITSC55140.2022.9921975. https://ieeexplore.ieee.org/document/9921975/

[7] Chen Y, Huang M, Tao Y. Density-based clustering multiple linear regression model of energy consumption for electric vehicles. Sustain Energy Technol Assess 2022;53:102614. https://doi.org/10.1016/j.seta.2022.102614. https://linkinghub.elsevier.com/retrieve/pii/S2213138822006646

[8] Chung J, Gulcehre C, Cho K, Bengio Y. Empirical evaluation of gated recurrent neural networks on sequence modeling. In: NIPS 2014 workshop on deep learning, December 2014; 2014.

[9] Chung YW, Khaki B, Li T, Chu C, Gadh R. Ensemble machine learning-based algorithm for electric vehicle user behavior prediction. Appl Energy 2019;254:113732. https://doi.org/10.1016/j.apenergy.2019.113732. https://linkinghub.elsevier.com/retrieve/pii/S0306261919314199

[10] Donkers A, Yang D, Viktorović M. Influence of driving style, infrastructure, weather and traffic on electric vehicle performance. Transp Res Part D Transp Environ 2020;88:102569. https://doi.org/10.1016/j.trd.2020.102569. https://linkinghub.elsevier.com/retrieve/pii/S1361920920307562

[11] Fetene GM, Kaplan S, Mabit SL, Jensen AF, Prato CG. Harnessing big data for estimating the energy consumption and driving range of electric vehicles. Transp Res Part D Transp Environ 2017;54:1–11. https://doi.org/10.1016/j.trd.2017.04.013. https://linkinghub.elsevier.com/retrieve/pii/S1361920917303188

[12] Fukushima A, Yano T, Imahara S, Aisu H, Shimokawa Y, Shibata Y. Prediction of energy consumption for new electric vehicle models by machine learning. IET Intell Transp Syst 2018;12:1174–80. https://doi.org/10.1049/iet-its.2018.5169. https://onlinelibrary.wiley.com/doi/10.1049/iet-its.2018.5169

[13] Gal Y, Ghahramani Z. Dropout as a BAYESIAN approximation: representing model uncertainty in deep learning. In: Proceedings of the 33rd International Conference on International Conference on machine Learning - volume 48; JMLR.org; 2016. p. 1050–9. Place: New York, NY, USA.

[14] Gao J, Yu B, Chen Y, Gao K, Bao S. A multi-perspective fusion model for operating speed prediction on highways using knowledge-enhanced graph neural networks. Comput Aided Civ Eng 2025;40:1004–27. https://doi.org/10.1111/mice.13382. https://onlinelibrary.wiley.com/doi/10.1111/mice.13382

[15] Guo J, Jiang Y, Liu C, Zhao D, Yu Y. Integrated multistep markov-based velocity predictor of energy consumption prediction model for battery electric vehicles. Transp B Transp Dyn 2021;9:399–414. https://doi.org/10.1080/21680566.2020.1867664. https://www.tandfonline.com/doi/full/10.1080/21680566.2020.1867664

[16] Hariharan C, Gunadevan D, Arun Prakash S, Latha K, Antony Aroul Raj V, Velraj R. Simulation of battery energy consumption in an electric car with traction and HVAC model for a given source and destination for reducing the range anxiety of the driver.

Energy 2022;249:123657. https://doi.org/10.1016/j.energy.2022.123657. https://www.sciencedirect.com/science/article/pii/S0360544222005606
[17] Hua Y, Sevegnani M, Yi D, Birnie A, McAslan S. Fine-grained RNN with transfer learning for energy consumption estimation on EVS. IEEE Trans Ind Informatics 2022;18:8182–90. https://doi.org/10.1109/TII.2022.3143155. https://ieeexplore.ieee.org/document/9682536/
[18] Huang H, He H, Wang Y, Zhang Z, Wang T. Energy consumption prediction of electric vehicles for data-scarce scenarios using pre-trained model. Transp Res Part D Transp Environ 2025;146:104830. https://doi.org/10.1016/j.trd.2025.104830. https://linkinghub.elsevier.com/retrieve/pii/S1361920925002408
[19] Huang HC, He HD, Peng ZR. Urban-scale estimation model of Carbon emissions for ride-hailing electric vehicles during operational phase. Energy 2024;293:130665. https://doi.org/10.1016/j.energy.2024.130665. https://linkinghub.elsevier.com/retrieve/pii/S0360544224004377
[20] Jankovic F, Scekic L, Mujovic S. Matlab/Simulink based energy consumption prediction of electric vehicles. In: 2021 21st International Symposium on Power Electronics (EE); Novi Sad, Serbia: IEEE; 2021. p. 1–5. https://doi.org/10.1109/Ee53374.2021.9628314. https://ieeexplore.ieee.org/document/9628314/
[21] Ji J, Bie Y, Zeng Z, Wang L. Trip energy consumption estimation for electric buses. Commun Transp Res 2022;2:100069. https://doi.org/10.1016/j.commtr.2022.100069. https://linkinghub.elsevier.com/retrieve/pii/S2772424722000191
[22] Krogh, B., Andersen, O., Torp, K., 2015. Analyzing Electric Vehicle Energy Consumption Using Very Large Data Sets, in: Renz, M., Shahabi, C., Zhou, X., Cheema, M.A. (Eds.), Database Systems for Advanced Applications. Springer International Publishing, Cham. volume 9050, pp. 471–487. URL: https://link.springer.com/10.1007/978-3-319-18123-3_28, doi:https://doi.org/10.1007/978-3-319-18123-3_28. series Title: Lecture Notes in Computer Science.
[23] Kolat M, Tettamanti T, Bécsi T, Esztergár-Kiss D. On the relationship between the activity at point of interests and road traffic. Commun Transp Res 2023;3:100102. https://doi.org/10.1016/j.commtr.2023.100102. https://linkinghub.elsevier.com/retrieve/pii/S2772424723000136
[24] Kuang S, Liu Y, Wang X, Wu X, Wei Y. Harnessing multimodal large language models for traffic knowledge graph generation and decision-making. Commun Transp Res 2024;4:100146. https://doi.org/10.1016/j.commtr.2024.100146. https://linkinghub.elsevier.com/retrieve/pii/S2772424724000295
[25] Kumari S, Ghosh S, Hota AR, Mukhopadhyay S. Energy consumption of electric vehicles: effect of lateral dynamics. In: 2023 IEEE 97th vehicular technology conference (vtc2023-Spring); Florence, Italy: IEEE; 2023. p. 1–5. https://doi.org/10.1109/VTC2023-Spring57618.2023.10200325. https://ieeexplore.ieee.org/document/10200325/
[26] Liu K, Wang J, Yamamoto T, Morikawa T. Exploring the interactive effects of ambient temperature and vehicle auxiliary loads on electric vehicle energy consumption. Appl Energy 2018;227:324–31. https://doi.org/10.1016/j.apenergy.2017.08.074. https://linkinghub.elsevier.com/retrieve/pii/S0306261917310929
[27] Liu Y, Jiang H, Yao R, Zhu H. Interpretable data-augmented adversarial variational autoencoder with sequential attention for imbalanced fault diagnosis. J Manuf Syst 2023;71:342–59. https://doi.org/10.1016/j.jmsy.2023.09.019. https://linkinghub.elsevier.com/retrieve/pii/S0278612523002017
[28] Maity A, Sarkar S. Data-driven probabilistic energy consumption estimation for battery electric vehicles with model uncertainty. Int J Green Energy 2023:1–18. https://doi.org/10.1080/15435075.2023.2276174. https://www.tandfonline.com/doi/full/10.1080/15435075.2023.2276174
[29] Mediouni H, Ezzouhri A, Charouh Z, El Harouri K, El Hani S, Ghogho M. Energy consumption prediction and analysis for electric vehicles: a hybrid approach. Energies 2022;15. https://doi.org/10.3390/en15176490. https://www.mdpi.com/1996-1073/15/17/6490
[30] Morlock F, Rolle B, Bauer M, Sawodny O. Forecasts of electric vehicle energy consumption based on characteristic speed profiles and real-time traffic data. IEEE Trans Veh Technol 2020;69:1404–18. https://doi.org/10.1109/TVT.2019.2957536. https://ieeexplore.ieee.org/document/8922762/
[31] Nam NT, Hung PD. Padding methods in convolutional sequence model: an application in Japanese handwriting recognition. In: Proceedings of the 3rd International Conference on machine Learning and soft Computing; Da Lat Viet Nam: ACM; 2019. p. 138–42. https://doi.org/10.1145/3310986.3310998. https://dl.acm.org/doi/10.1145/3310986.3310998
[32] Oh G, Leblanc DJ, Peng H. Vehicle energy dataset (VED), a large-scale dataset for vehicle energy consumption research. IEEE Trans Intell Transp Syst 2022;23:3302–12. https://doi.org/10.1109/TITS.2020.3035596. https://ieeexplore.ieee.org/document/9262035/
[33] Pan Y, Fang W, Zhang W. Development of an energy consumption prediction model for battery electric vehicles in real-world driving: a combined approach of short-trip segment division and deep learning. J Clean Prod 2023;400:136742. https://doi.org/10.1016/j.jclepro.2023.136742. https://linkinghub.elsevier.com/retrieve/pii/S0959652623009009
[34] Petkevicius L, Saltenis S, Civilis A, Torp K. Probabilistic deep learning for electric-vehicle energy-use prediction. In: 17th international symposium on spatial and temporal databases; virtual USA: ACM; 2021. p. 85–95. https://doi.org/10.1145/3469830.3470915. https://dl.acm.org/doi/10.1145/3469830.3470915
[35] Qi X, Wu G, Boriboonsomsin K, Barth MJ. Data-driven decomposition analysis and estimation of link-level electric vehicle energy consumption under real-world traffic conditions. Transp Res Part D Transp Environ 2018;64:36–52. https://doi.org/10.1016/j.trd.2017.08.008. https://linkinghub.elsevier.com/retrieve/pii/S1361920916307714
[36] Shen H, Zhou X, Ahn H, Lamantia M, Chen P, Wang J. Personalized velocity and energy prediction for electric vehicles with road features in consideration. IEEE Trans Transp Electr 2023;9:3958–69. https://doi.org/10.1109/TTE.2023.3241098. https://ieeexplore.ieee.org/document/10032579/
[37] Sun T, Xu Y, Feng L, Xu B, Chen D, Zhang F, et al. A vehicle-cloud collaboration strategy for remaining driving range estimation based on online traffic route information and future operation condition prediction. Energy 2022;248:123608. https://doi.org/10.1016/j.energy.2022.123608. https://linkinghub.elsevier.com/retrieve/pii/S0360544222005114
[38] Tran TB, Kolmanovsky I, Biberstein E, Makke O, Tharayil M, Gusikhin O. Wind sensitivity of electric vehicle energy consumption and influence on range prediction and optimal vehicle routes. In: 2023 IEEE International Conference on Mobility, operations, services and technologies (MOST); Detroit, MI, USA: IEEE; 2023. p. 112–23. https://doi.org/10.1109/MOST57249.2023.00020. https://ieeexplore.ieee.org/document/10210889/
[39] Ullah I, Liu K, Yamamoto T, Al Mamlook RE, Jamal A. A comparative performance of machine learning algorithm to predict electric vehicles energy consumption: a path towards sustainability. Energy Environ 2022;33:1583–612. https://doi.org/10.1177/0958305X211044998. http://journals.sagepub.com/doi/10.1177/0958305X211044998
[40] Ullah I, Liu K, Yamamoto T, Zahid M, Jamal A. Electric vehicle energy consumption prediction using stacked generalization: an ensemble learning approach. Int J Green Energy 2021;18:896–909. https://doi.org/10.1080/15435075.2021.1881902. https://www.tandfonline.com/doi/full/10.1080/15435075.2021.1881902
[41] Vepsäläinen J, Otto K, Lajunen A, Tammi K. Computationally efficient model for energy demand prediction of electric city bus in varying operating conditions. Energy 2019;169:433–43. https://doi.org/10.1016/j.energy.2018.12.064. https://linkinghub.elsevier.com/retrieve/pii/S0360544218324307
[42] Wang S, Gao K, Zhang L, Liu Y, Chen L. Probabilistic prediction of longitudinal trajectory considering driving heterogeneity with interpretability. IEEE Intell Transp Syst Mag 2024:2–18. https://doi.org/10.1109/MITS.2024.3399597. https://ieeexplore.ieee.org/document/10542992/
[43] Wang S, Gao K, Zhang L, Yu B, Easa SM. Geographically weighted machine learning for modeling spatial heterogeneity in traffic crash frequency and determinants in US. Accid Anal Prev 2024;199:107528. https://doi.org/10.1016/j.aap.2024.107528. https://linkinghub.elsevier.com/retrieve/pii/S0001457524000733
[44] Xu X, Aziz HA, Liu H, Rodgers MO, Guensler R. A scalable energy modeling framework for electric vehicles in regional transportation networks. Appl Energy 2020;269:115095. https://doi.org/10.1016/j.apenergy.2020.115095. https://www.sciencedirect.com/science/article/pii/S0306261920306073
[45] Yan H, Tang X. Incorporating range anxiety into electric vehicle highway charging decisions: a Bayesian game analysis. In: Proceedings of the 14th ACM International Conference on Future Energy Systems; Orlando FL USA: ACM; 2023. p. 184–8. https://doi.org/10.1145/3575813.3595195. https://dl.acm.org/doi/10.1145/3575813.3595195
[46] Zhang J, Wang Z, Liu P, Zhang Z. Energy consumption analysis and prediction of electric vehicles based on real-world driving data. Appl Energy 2020;275:115408. https://doi.org/10.1016/j.apenergy.2020.115408. https://linkinghub.elsevier.com/retrieve/pii/S030626192030920X
[47] Zhang Q, Tian S. Energy consumption prediction and control algorithm for hybrid electric vehicles based on an equivalent minimum fuel consumption model. Sustainability 2023;15:9394. https://doi.org/10.3390/su15129394. https://www.mdpi.com/2071-1050/15/12/9394
[48] Zhang S, Fatih D, Abdulqadir F, Schwarz T, Ma X. Extended vehicle energy dataset (EVED): an enhanced large-scale dataset for deep learning on vehicle trip energy consumption; 2022 URL: https://arxiv.org/abs/2203.08630, https://doi.org/10.48550/ARXIV.2203.08630. publisher: arXiv Version Number: 1.
[49] Zhao Y, Wang Z, Shen ZJM, Zhang L, Dorrell DG, Sun F. Big data-driven decoupling framework enabling quantitative assessments of electric vehicle performance degradation. Appl Energy 2022;327:120083. https://doi.org/10.1016/j.apenergy.2022.120083. https://linkinghub.elsevier.com/retrieve/pii/S030626192201340X
[50] Çeven S, Albayrak A, Bayir R. Real-time range estimation in electric vehicles using fuzzy logic classifier. Comput Electr Eng 2020;83:106577. https://doi.org/10.1016/j.compeleceng.2020.106577. https://linkinghub.elsevier.com/retrieve/pii/S0045790619318786